

## Insights Into Targeting the SARS-CoV-2: Design, Synthesis, *In Silico* Studies and Antiviral Evaluation of New Dimethylxanthine Derivatives

(Supplementary Materials)

Abdalla R. Mohamed <sup>a,\*</sup>, Ahmed Mostafa <sup>b</sup>, Mahmoud A. El Hassab <sup>c</sup>, Gomaa M. Hedeab <sup>d,e</sup>, Sara H. Mahmoud <sup>b</sup>, Riham F. George <sup>f</sup>, Hanan H. Georgey <sup>f,g</sup>, Nagwa M. Abdel Gawad <sup>f</sup>, Mohamed K. El-Ashrey <sup>c,f</sup>

<sup>a</sup> Pharmaceutical Chemistry Department, Faculty of Pharmacy, Egyptian Russian University, Badr City, Cairo 11829, Egypt.

<sup>b</sup> Center of Scientific Excellence for Influenza Viruses, National Research Centre, Giza 12622, Egypt.

<sup>c</sup> Medicinal Chemistry Department, Faculty of Pharmacy, King Salman International University, Ras-Sedr, South Sinai, Egypt.

<sup>d</sup> Pharmacology Department and Health Research Unit, Medical College, Jouf University, KSA.

<sup>e</sup> Pharmacology Department, Faculty of Medicine, Beni-Suef University, Egypt.

<sup>f</sup> Pharmaceutical Chemistry Department, Faculty of Pharmacy, Cairo University, Cairo 11562, Egypt.

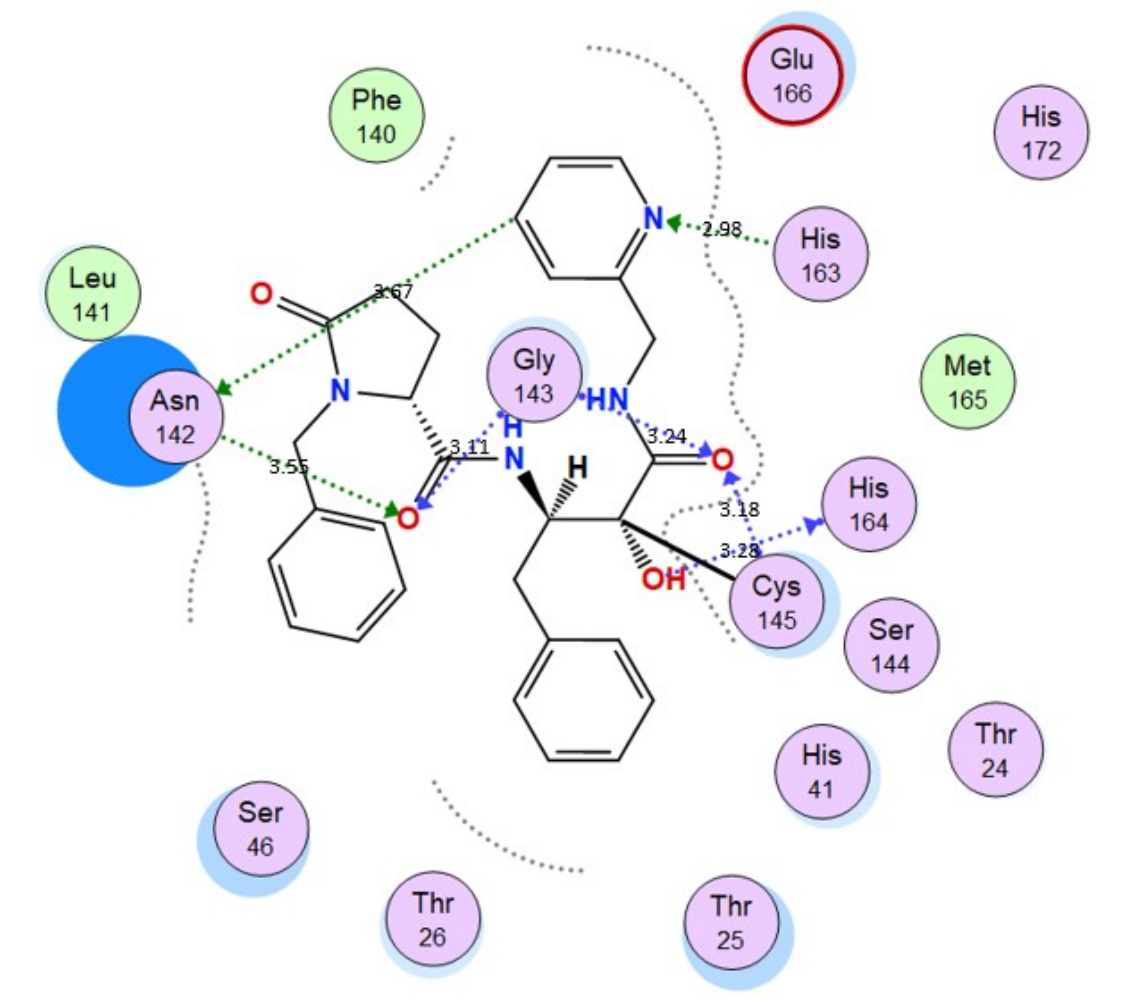
<sup>g</sup> Pharmaceutical Chemistry Department, Faculty of Pharmacy and Drug Technology, Egyptian Chinese University, 11786, Cairo, Egypt.

### Content

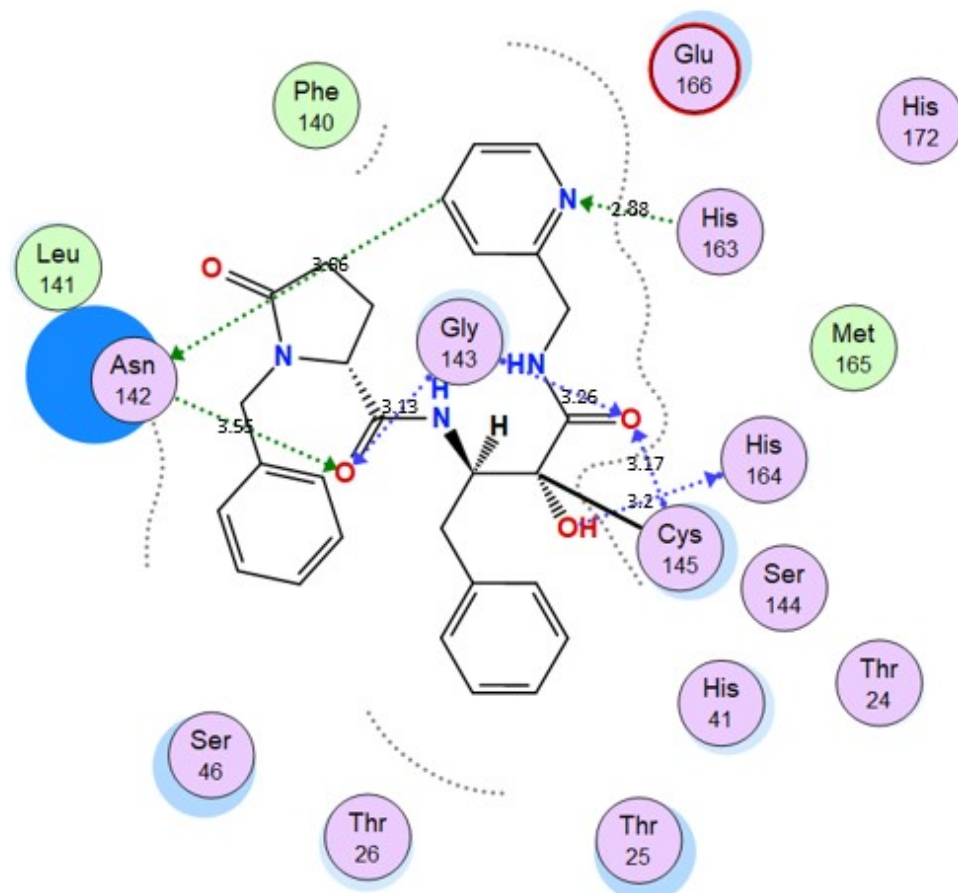
<b>1. Molecular Docking</b>	<b>1</b>
<b>2. Density functional theory (DFT) calculations</b>	<b>13</b>
<b>3. MM-PBSA calculations</b>	<b>15</b>
<b>4. Hydrogen bond analysis upon time evolution</b>	<b>15</b>
<b>5. NCI-60 cell lines panel</b>	<b>19</b>
<b>6. Oral toxicity prediction of compounds 5, 9a and 19</b>	<b>21</b>
<b>7. Spectral data</b>	<b>27</b>
<b>References</b>	<b>41</b>

## 1. Molecular Docking

Docking validation of the co-crystallized ligand, in the SARS-CoV-2 M<sub>pro</sub> (PDB ID: 7AEH) active site



(A)



(B)

**Figure 1S.** (A) 2D interaction diagram showing ligand docking pose interactions with the key amino acids (hot spots) in the  $M_{pro}$  active site (Distance in Å). (B) 2D diagram of the docking pose in  $M_{pro}$  active site with RMSD of 0.75 Å.

Docking validation of the co-crystallized ligand, in the SARS-CoV-2 RdRp (PDB ID: 7BV2) active site



(B)

**Figure 2S.** (A) 2D interaction diagram showing ligand docking pose interactions with the key amino acids (hot spots) in the RdRp active site (Distance in Å). (B) 2D diagram of the docking pose in RdRp active site with RMSD of 0.56 Å.

**Table 1S.** Docking scores of the tested compounds in  $M_{\text{pro}}$  & RdRp.

Compound	$M_{\text{PRO}}$ binding score (Kcal/mol)	RdRp binding score (Kcal/mol)
<b>3</b>	-15.23	-11.88
<b>5</b>	-15.90	-12.70
<b>9a</b>	-17.52	-13.72
<b>9b</b>	-16.50	-12.53
<b>12a</b>	-15.11	-11.96
<b>12b</b>	-16.01	-12.29
<b>14</b>	-14.90	-10.70
<b>15a</b>	-14.47	-10.98
<b>15b</b>	-16.43	-11.55
<b>19</b>	-16.57	-13.10

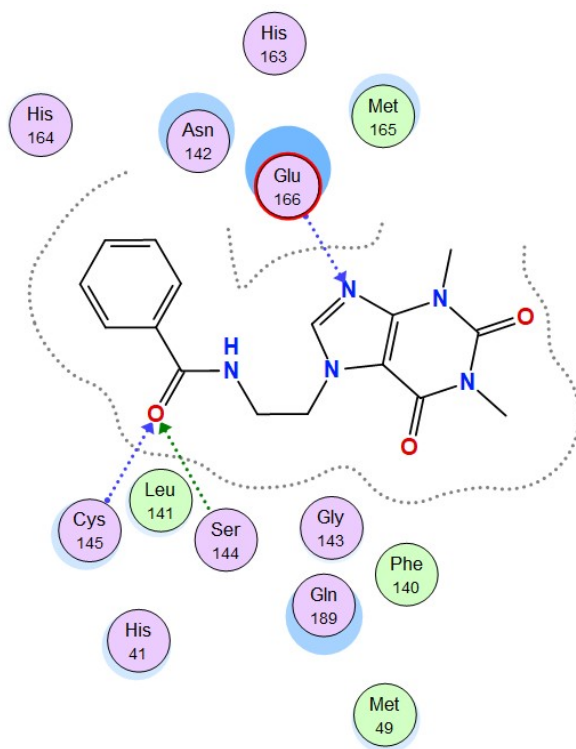


**Figure 3S.** 2D interaction of compound **3** in  $M_{\text{pro}}$  active site

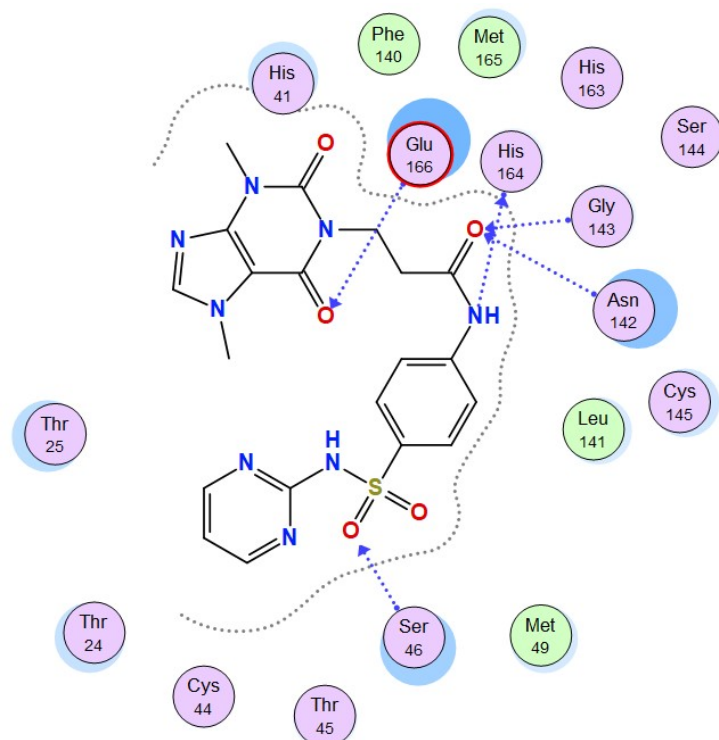


**Figure 4S.** 2D interaction of compound **9b** in  $M_{\text{pro}}$  active site

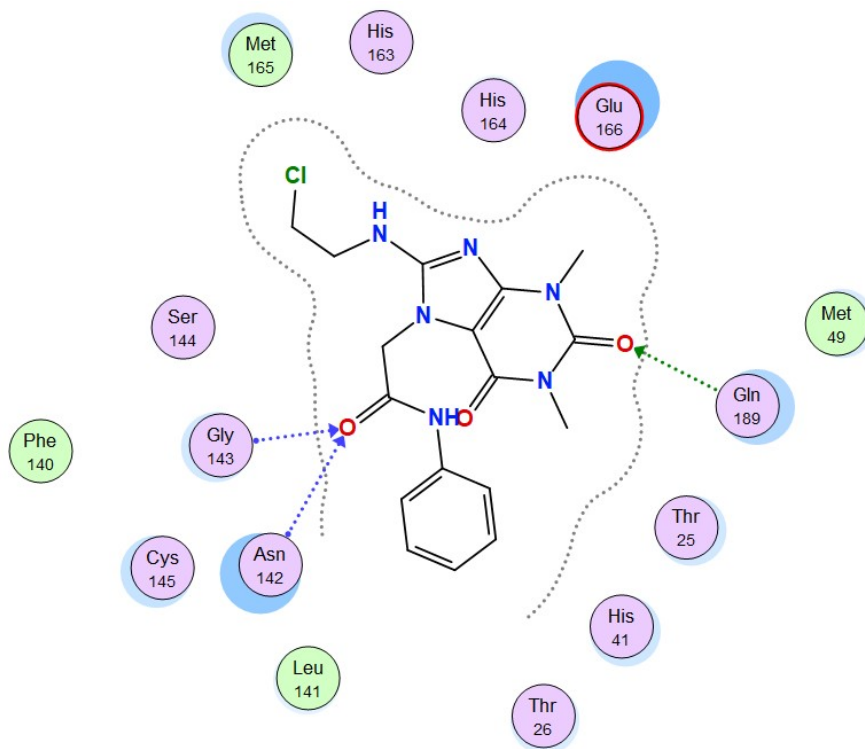


**Figure 5S.** 2D interaction of compound **12a** in  $M_{\text{pro}}$  active site

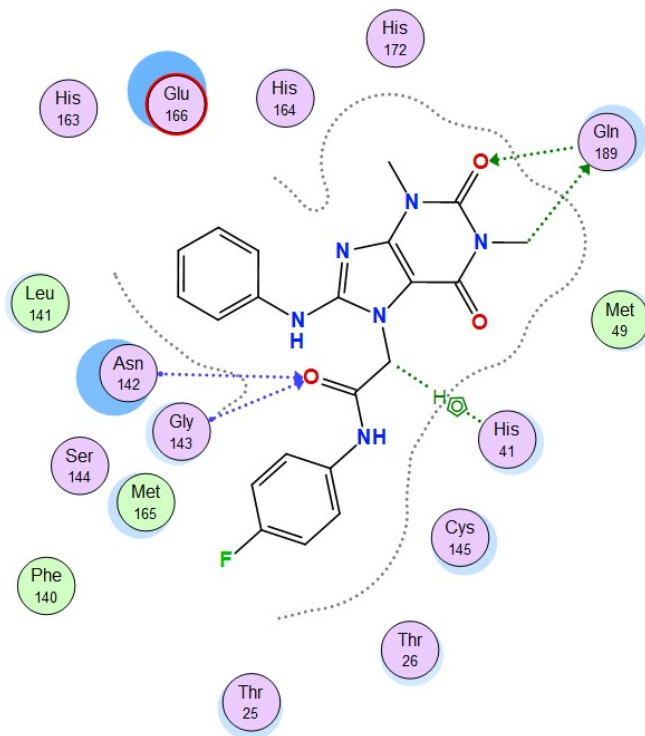


**Figure 6S.** 2D interaction of compound **12b** in  $M_{pro}$  active site

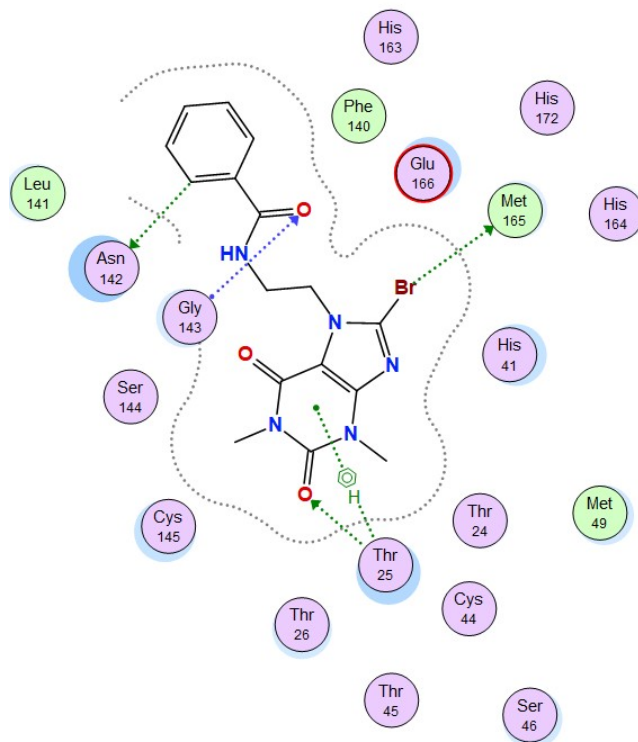


**Figure 7S.** 2D interaction of compound **14** in  $M_{pro}$  active site

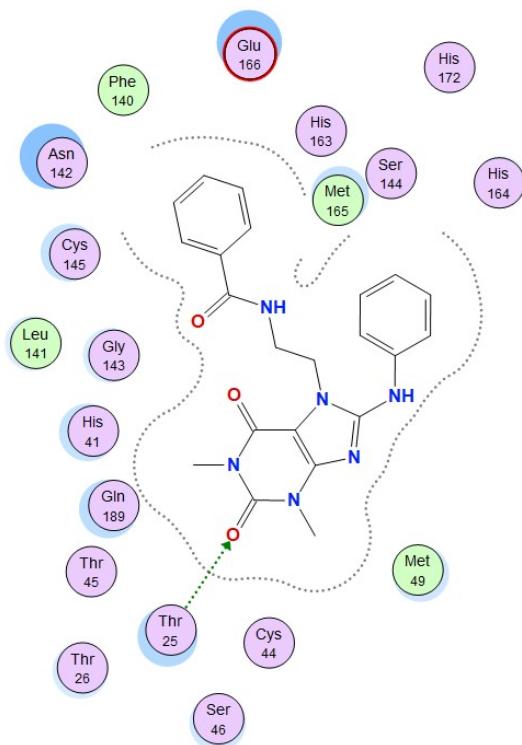


**Figure 8S.** 2D interaction of compound **15a** in M<sub>pro</sub> active site

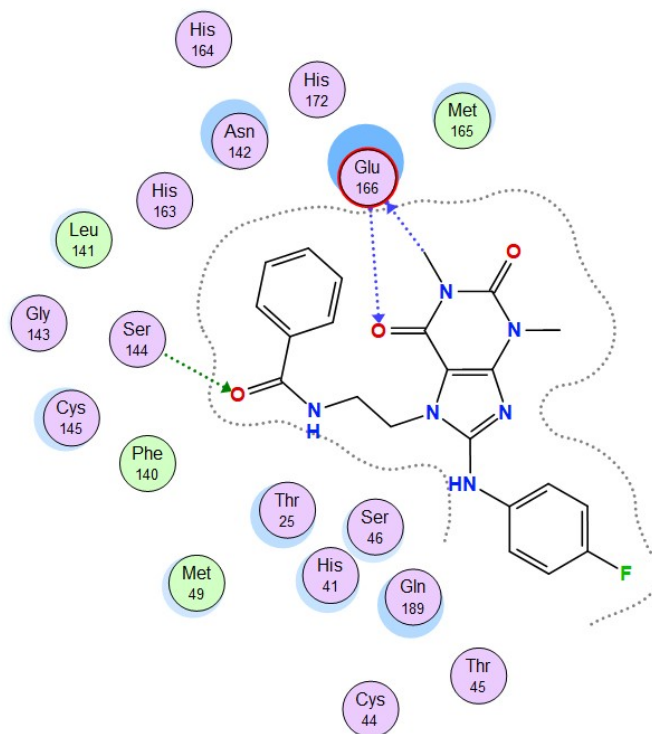


**Figure 9S.** 2D interaction of compound **15b** in M<sub>pro</sub> active site



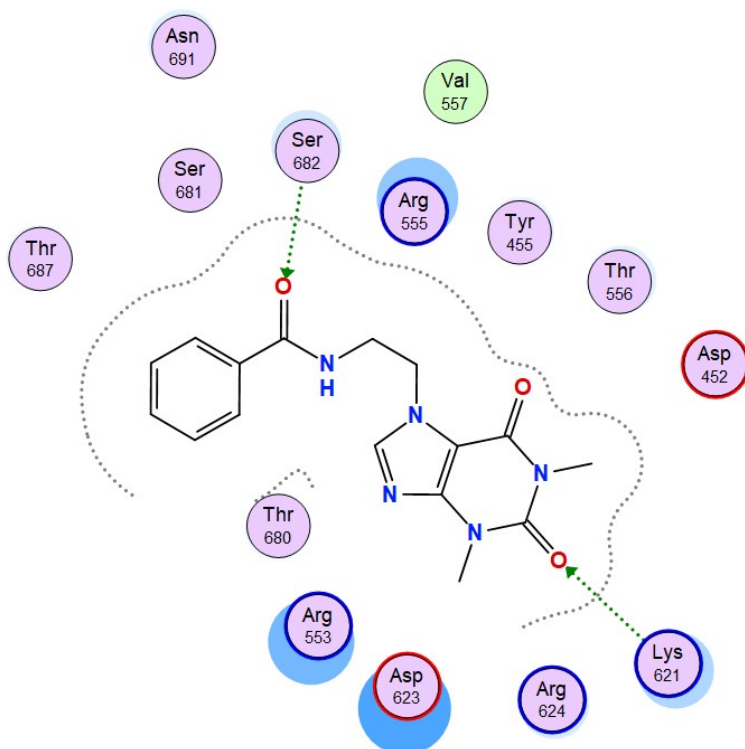


**Figure 10S.** 2D interaction of compound **3** in RdRp active site

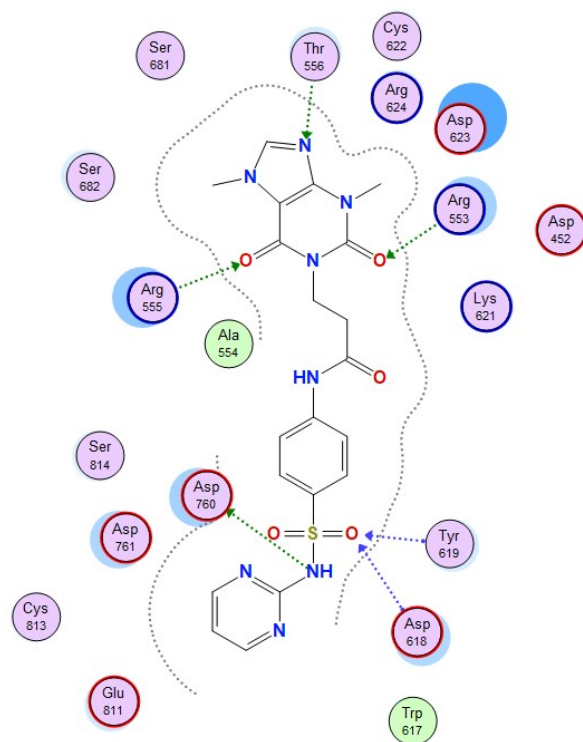


**Figure 11S.** 2D interaction of compound **9b** in RdRp active site

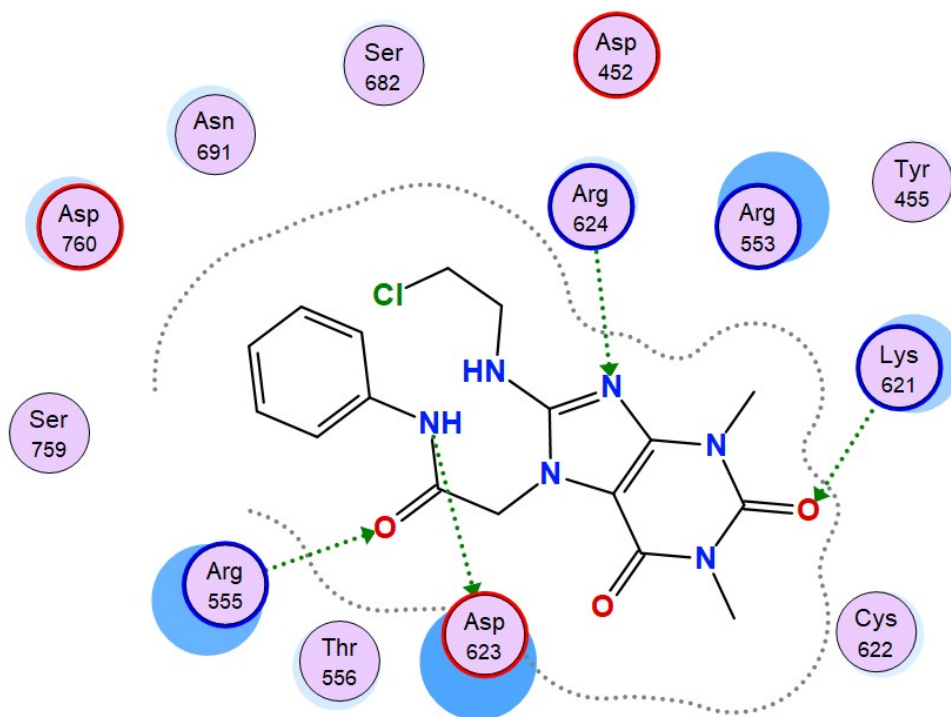


**Figure 12S.** 2D interaction of compound **12a** in RdRp active site

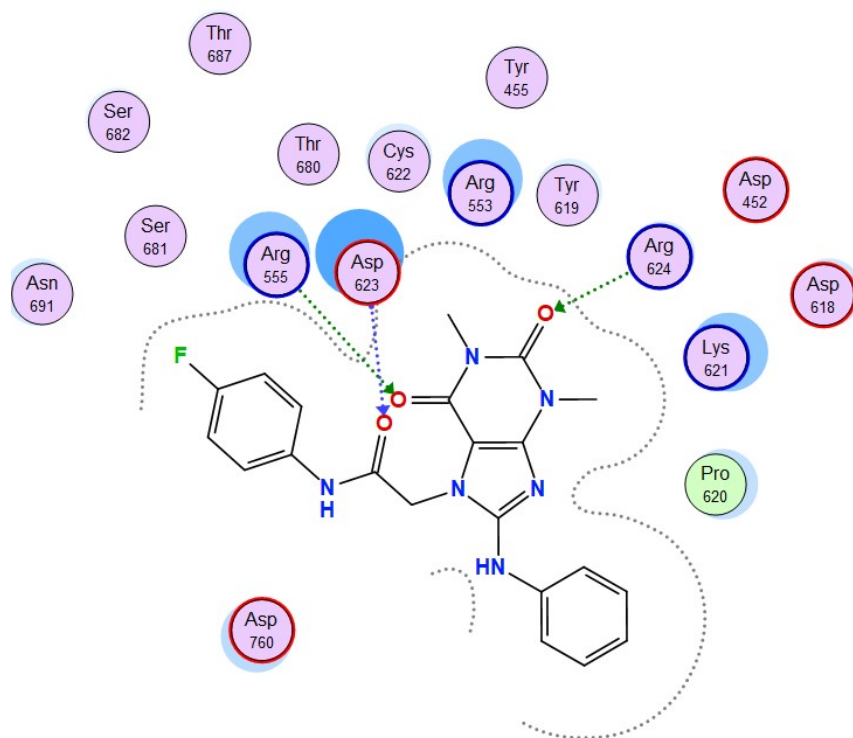


**Figure 13S.** 2D interaction of compound **12b** in RdRp active site

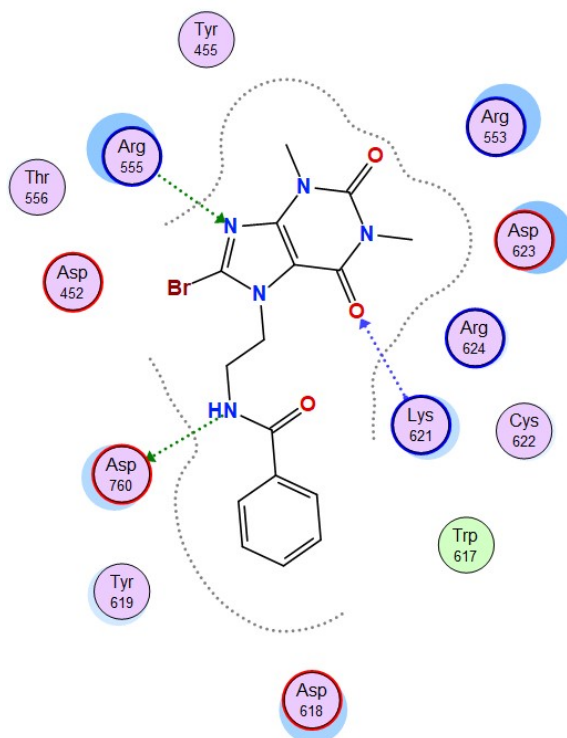


**Figure 14S.** 2D interaction of compound **14** in RdRp active site

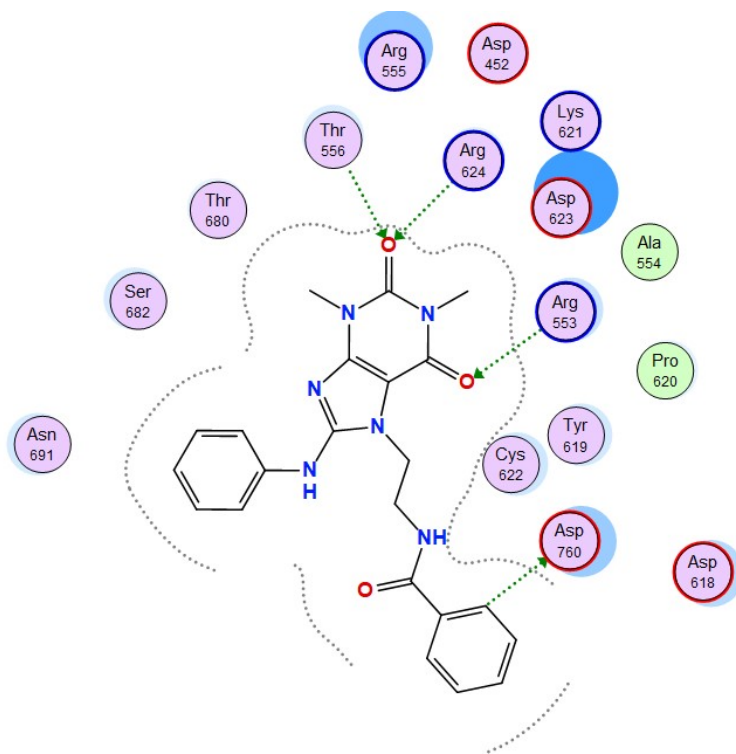


**Figure 15S.** 2D interaction of compound **15a** in RdRp active site

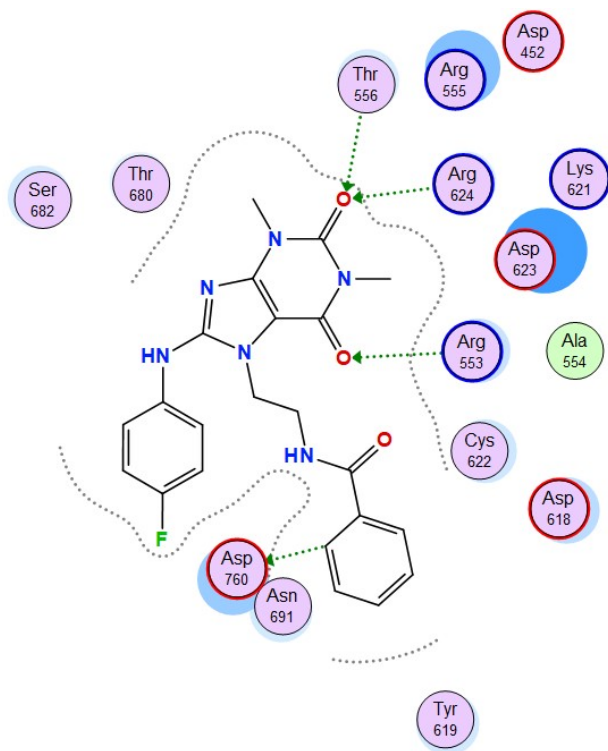


**Figure 16S.** 2D interaction of compound **15b** in RdRp active site

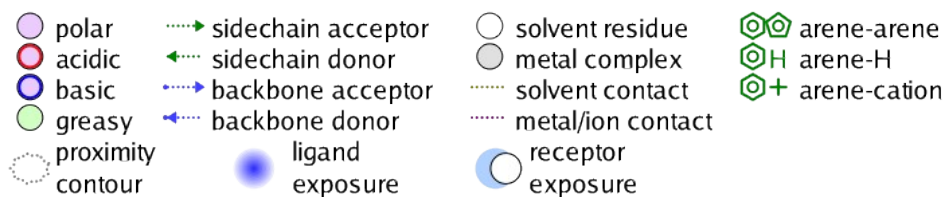


**Figure 17S.** A legend guide to binding interactions regarding all the performed docking studies.

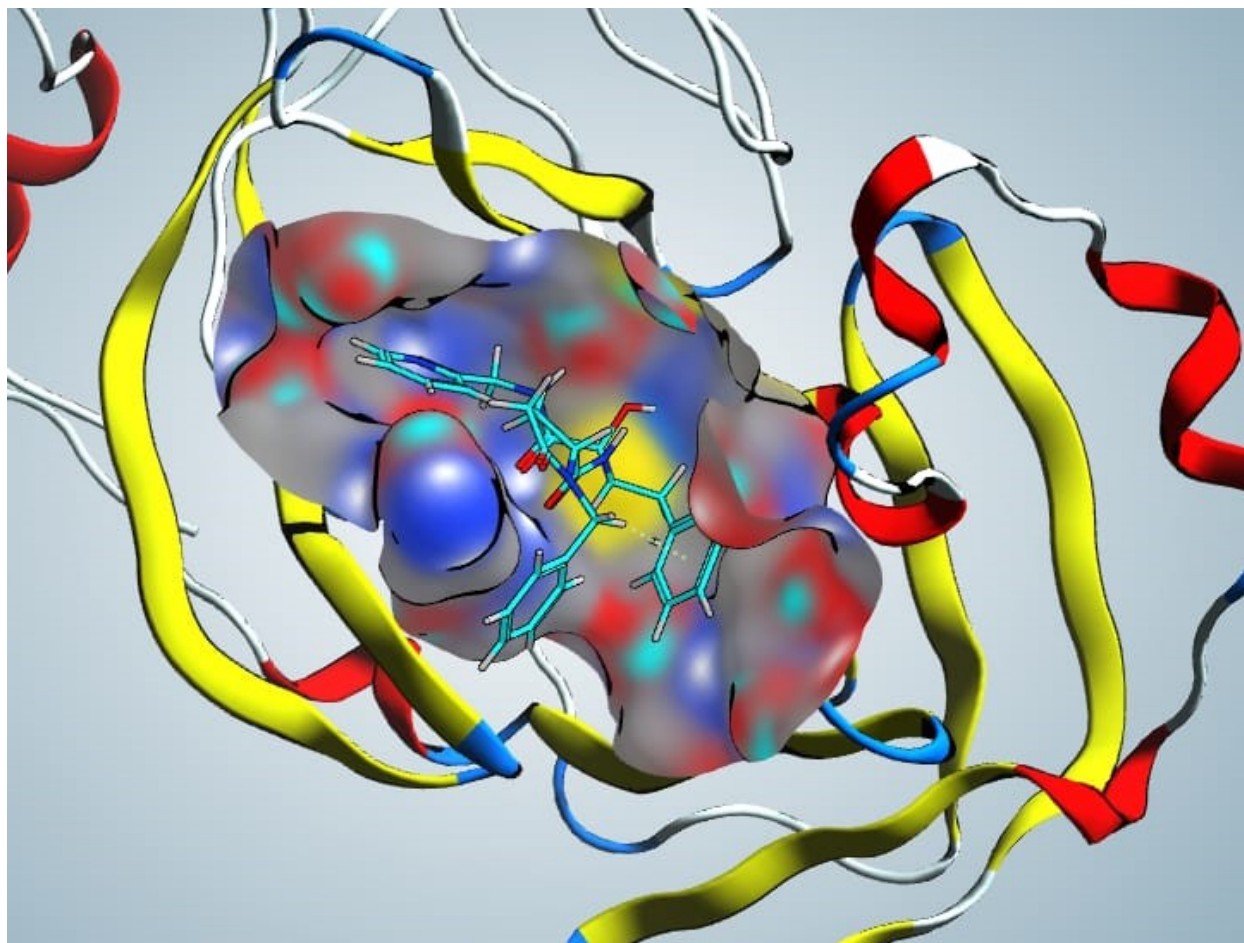


**Figure 18S.** 3D presentation of surface and map of SARS-CoV-2 M<sub>pro</sub> active site (PDB ID: 7AEH) with compound **9a**.

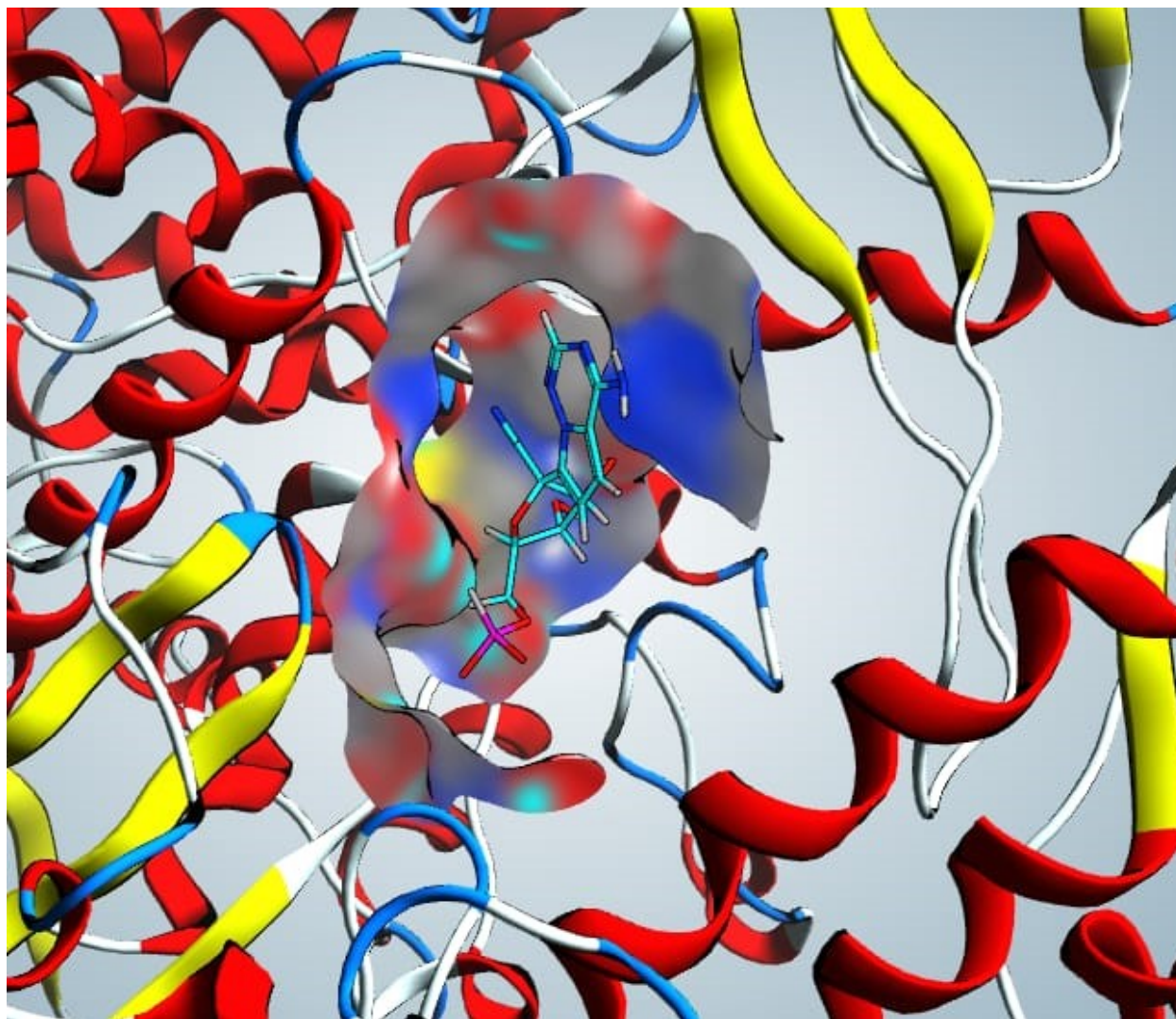
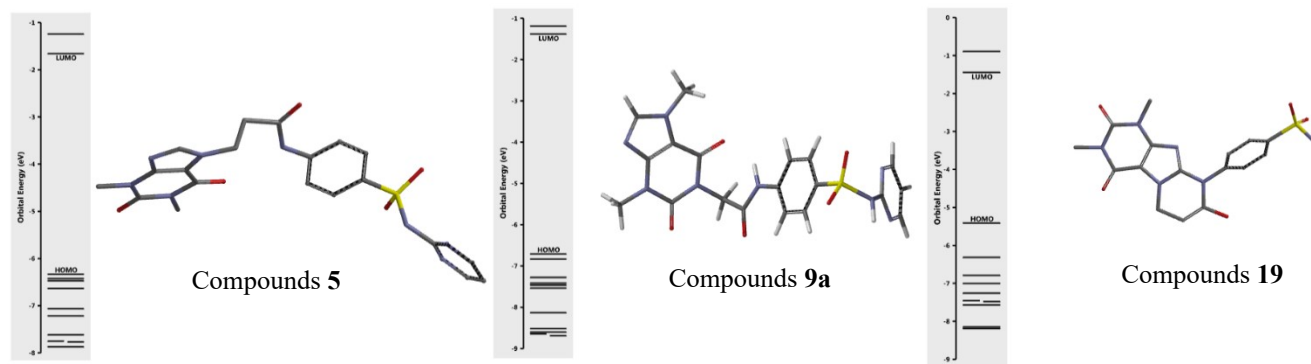


**Figure 19S.** 3D presentation of surface and map of SARS-CoV-2 RdRp active site (PDB ID: 7BV2) with compound **9a**.

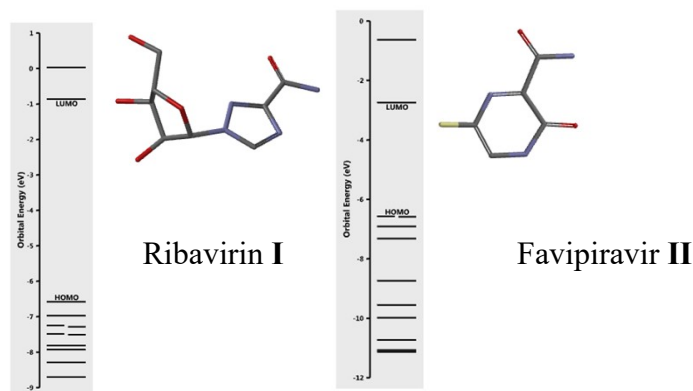
## 2. Density functional theory (DFT) calculations

According to the performed docking studies, compounds **9a**, **19** and **5** were predicted to have interesting binding modes in the active site of SARS-CoV-2  $M_{pro}$  and RdRp enzymes. Quantum chemical computations using the DFT/B3LYP approach with 6-311G++(d,p) basis set were utilized to get insights regarding the energy values of compounds **9a**, **19** and **5** (**Table 2S**) [1]. **Figure 20S-A** represents the optimized structures along with their HOMO and LUMO values. The DFT calculations revealed favorable energetic parameters for the three compounds, and particularly, compound **9a** was comparable with compounds **I** and **II** (**Figure 20S-B**).

## Supplementary Materials



(A)



(B)

**Figure 20S.** (A) DFT calculations for compounds **5**, **9a** and **19**. (B) The most stable conformation of Ribavirin I and Favipiravir II according to DFT calculation [2, 3].

**Table 2S.** The molecular properties of compounds **5**, **9a** and **19** after DFT calculations

Compound	Energy (a.u.)	Energy solvation (Kj/Mol)	E HOMO (eV)	E LUMO (eV)	Dipole Moment (Debye)	No. of conformers	% Of the most favorable conformer
<b>5</b>	-1985.50614	-143.63	-6.33	-1.66	8.11	1296	99.993
<b>9a</b>	-1946.20887	-125.68	-6.71	-1.38	9.11	216	99.989
<b>19</b>	-1721.30460	-112.69	-5.41	-1.45	8.50	24	99.601

The Spartan '14 program was used to perform the quantum chemistry calculations using the DFT method. Spartan '14 was used to display all of the data files. DFT at 6-311G++(d,p) basis set/B3LYP approach was utilized to optimize organic chemical structure of compound **5**, **9a** and **19** [1].

### 3. MM-PBSA calculations

The total free energy of any of the three mentioned entities (complex, receptor and ligand) were calculated for all MD trajectories from its molecular mechanics potential energy plus the energy of the solvation, using the g\_mmpbsa package. The following formula was used.

$$\Delta G_{(\text{Binding})} = G_{(\text{Complex})} - G_{(\text{Receptor})} - G_{(\text{Ligand})}$$

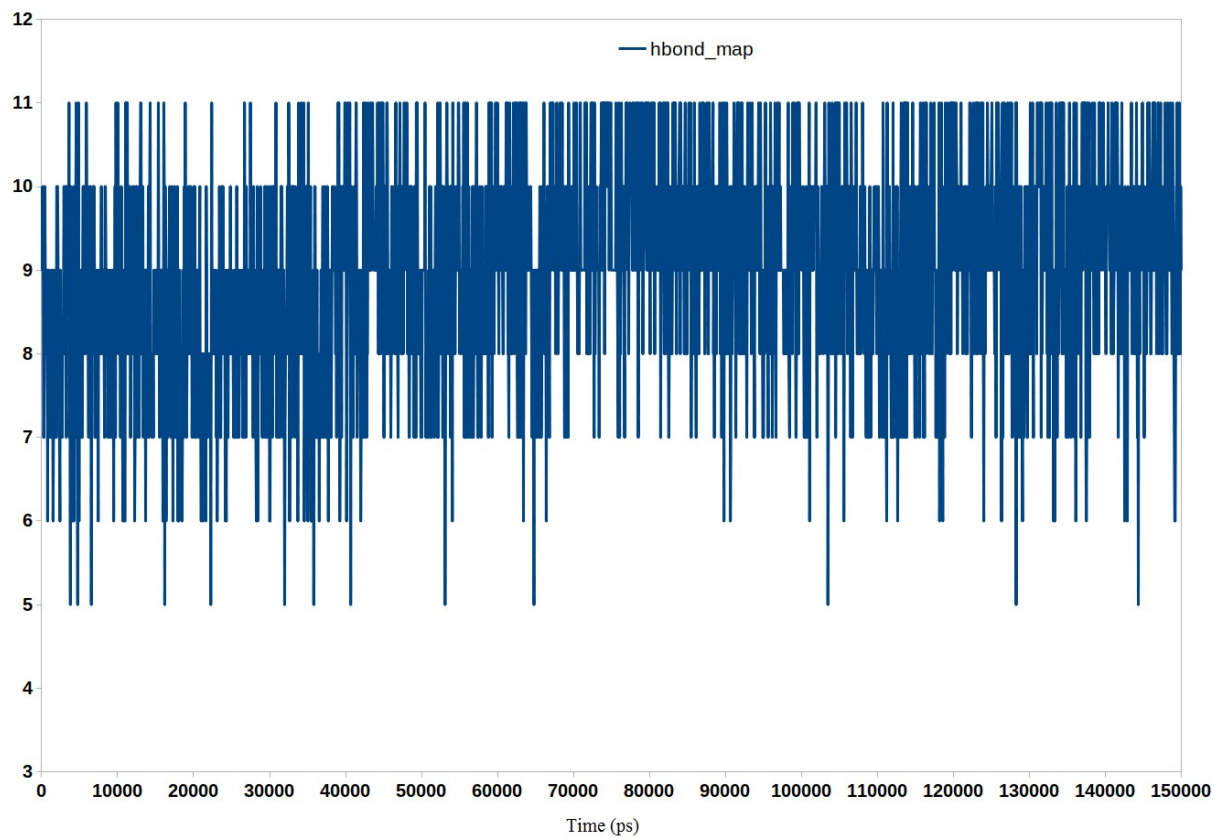
Where  $G_{(\text{Complex})}$  is the total free energy of the protein–ligand complex,  $G_{(\text{Receptor})}$  and  $G_{(\text{Ligand})}$  are the total free energies of the isolated protein and ligand in solvent, respectively. Individual energies along with the values of standard deviations were calculated and then summed together to yield the average total free energy of each component. Finally, to calculate the binding-free energy, the total free energy of the receptor and the ligand were subtracted from the total free energy of the complex [4].

### 4. Hydrogen bond analysis upon time evolution

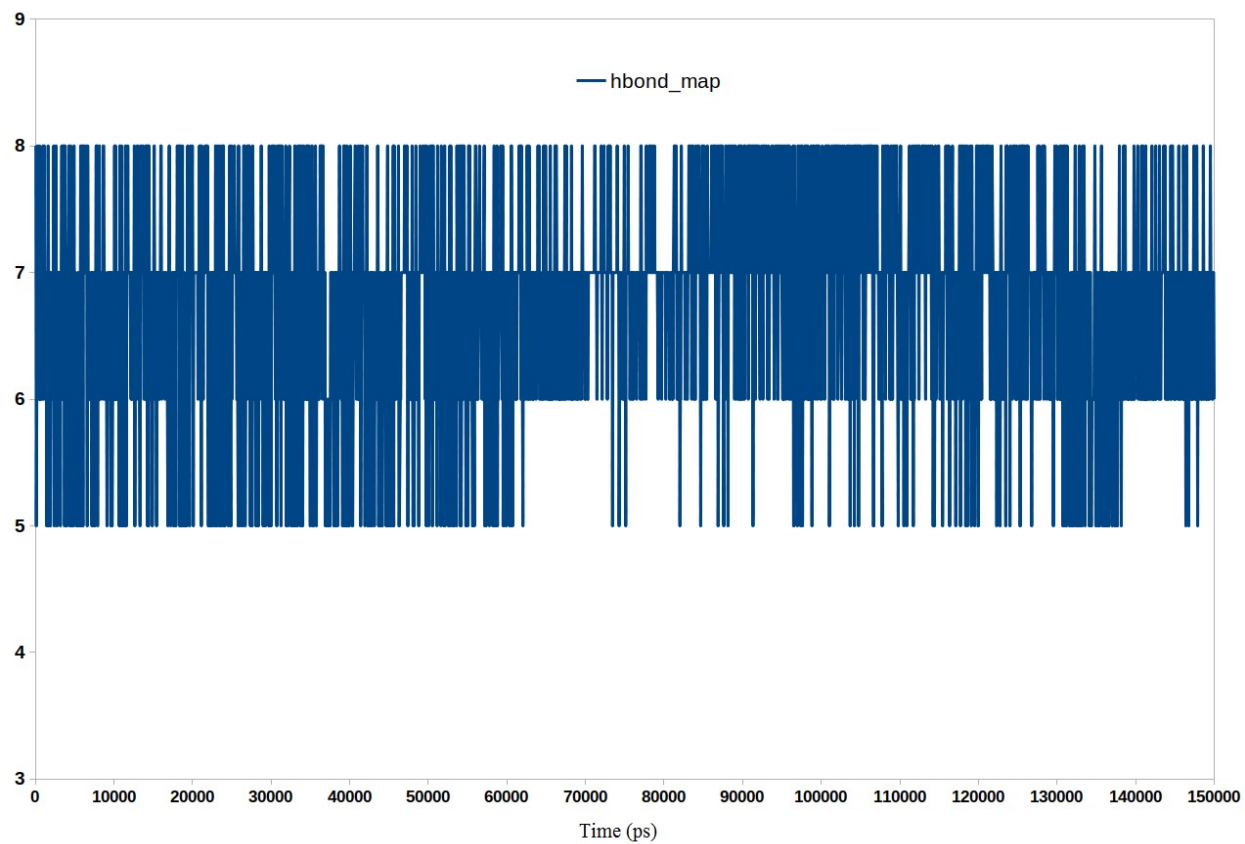
For further insights into the binding process between compound **9a** and the active sites of  $M_{\text{pro}}$  and RdRp enzymes, hydrogen bond interactions during the MDS were analyzed using VMD 1.8.2 program [5]. As **Figure 21S-A** and **B** demonstrate, compound **9a** was able to form multiple hydrogen bond interactions with the  $M_{\text{pro}}$  and RdRp enzymes, respectively, throughout the entire MDS. Furthermore, the binding interactions between compound **9a** and both of  $M_{\text{pro}}$  or RdRp induced stable complexes as revealed from **Figure 22S-A** and **B**.



# Supplementary Materials

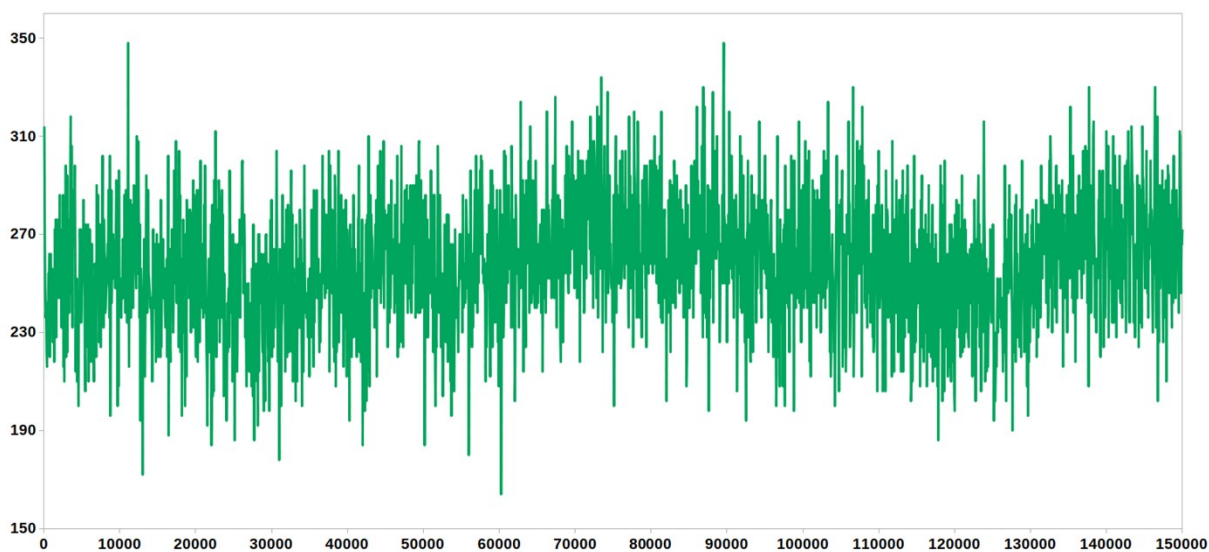


(A)

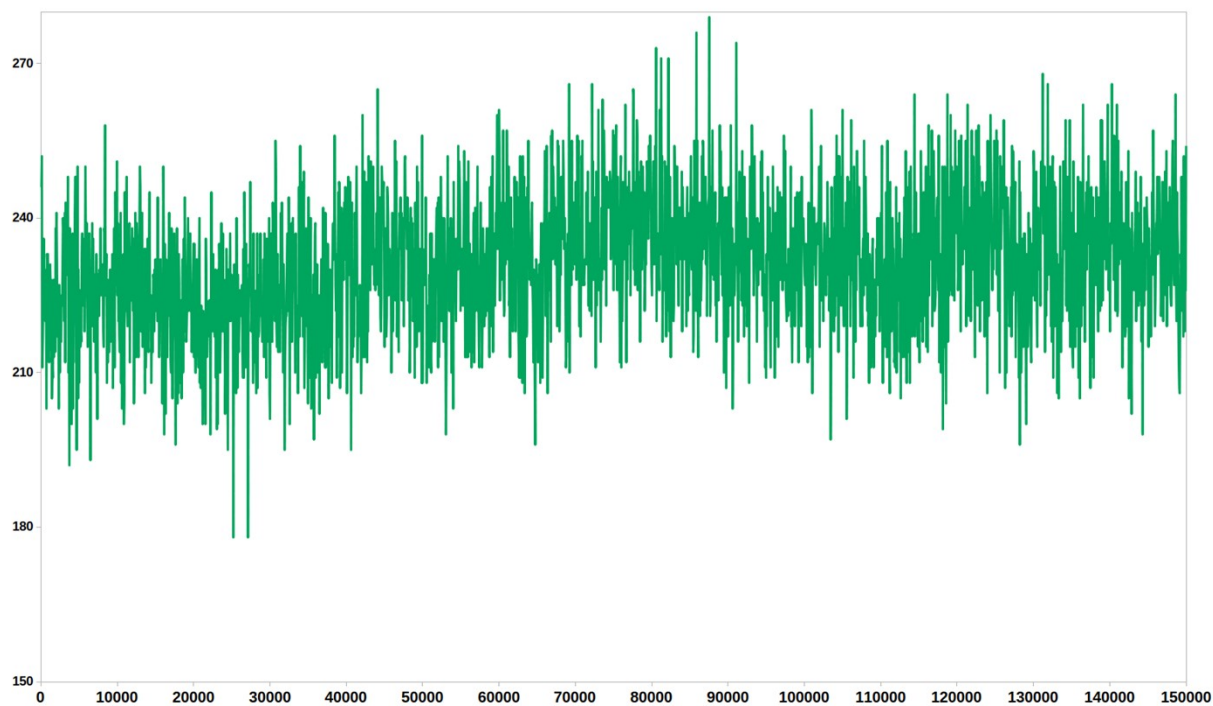


(B)

**Figure 21S.** The hydrogen bond contacts during the entire MDS; (A) compound **9a** with  $M_{\text{pro}}$ , (B) compound **9a** with RdRp.



(A)



(B)

**Figure 22S.** The hydrogen bond contacts during the entire MDS; (A)  $M_{\text{pro}}$  enzyme (B) RdRp enzyme.

## 5. NCI-60 cell lines panel

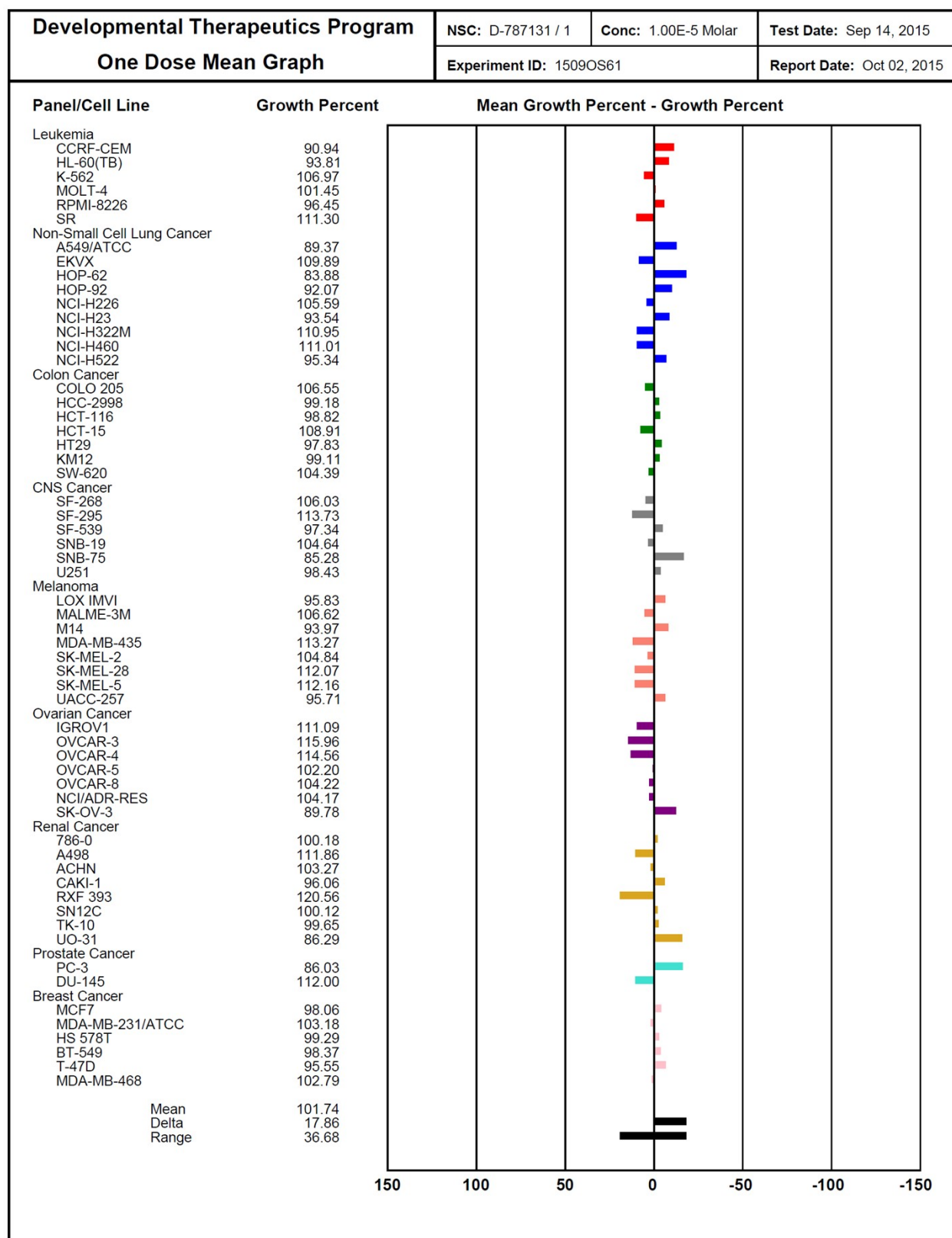


Figure. 23S. NCI-60 cell line panel of compound 5

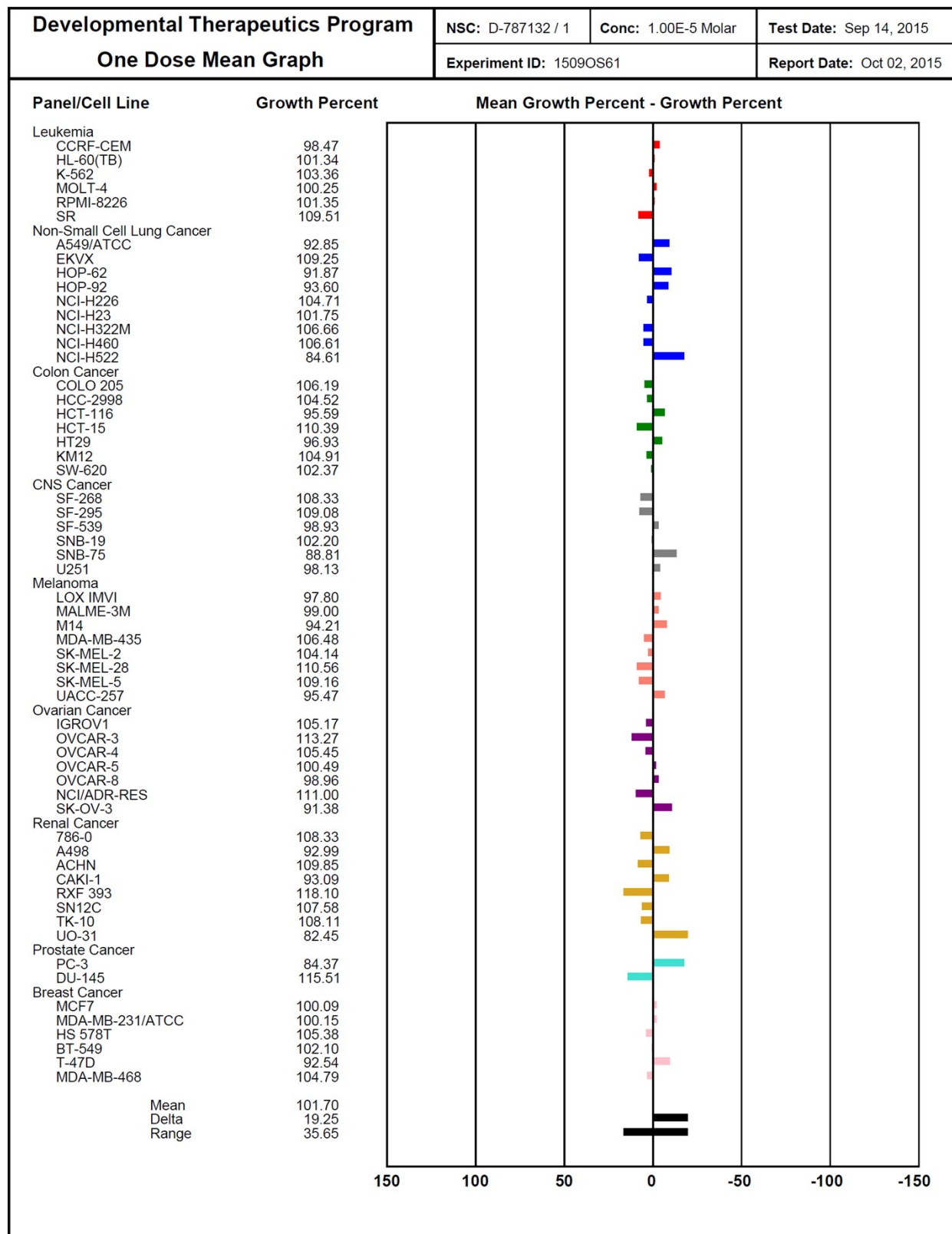


Figure. 24S. NCI-60 cell line panel of compound 9a

## 6. Oral toxicity prediction of compounds 5, 9a and 19

Table 3S. *In silico* oral toxicity prediction for compounds 5, 9a and 19

Compound	LD <sub>50</sub> (mg/kg)	Predicted Toxicity Class <sup>a</sup>	Average similarity (%)	Prediction accuracy (%)
<b>5</b>	300	3	60.56	68.07
<b>9a</b>	598	4	60.75	68.07
<b>19</b>	500	4	47.93	54.26
<b>Remdesivir</b>	1000	4	40.93	54.26
<b>Favipiravir</b>	1717	4	39.16	23.00

<sup>a</sup> Toxicity Class ranging from 1 to 6 according to the Global Harmony System (GHS) [6].

The ProTox web server was used to estimate rodent oral toxicity and indication of possible toxicity targets for compounds **5**, **9a** and **19** as reported previously [6]. As seen in **Table 3S**, the evaluated LD<sub>50</sub> was ranged from 300 to 598 mg/kg for the predicted compounds. The evaluated molecules were predicted to be in toxicity classes of 3 or 4, and have no toxic fragments. Furthermore, the submitted compounds were found to be not binding to toxic targets, only compound 19 was found to have a probable hepatotoxicity, figures S-S.

Molweight	484.49
Number of hydrogen bond acceptors	30
Number of hydrogen bond donors	2
Number of atoms	54
Number of bonds	57
Number of rotatable bonds	8
Molecular refractivity	123.38
Topological Polar Surface Area	171.25
octanol/water partition coefficient(logP)	1.28

(A)

## Supplementary Materials

Classification	Target	Shorthand	Prediction	Probability
Organ toxicity	Hepatotoxicity	dili	Inactive	0.52
Toxicity end points	Carcinogenicity	carcino	Inactive	0.61
Toxicity end points	Immunotoxicity	immuno	Inactive	0.99
Toxicity end points	Mutagenicity	mutagen	Inactive	0.76
Toxicity end points	Cytotoxicity	cyto	Inactive	0.56
Tox21-Nuclear receptor signalling pathways	Aryl hydrocarbon Receptor (AhR)	nr_ahr	Inactive	0.92
Tox21-Nuclear receptor signalling pathways	Androgen Receptor (AR)	nr_ar	Inactive	0.97
Tox21-Nuclear receptor signalling pathways	Androgen Receptor Ligand Binding Domain (AR-LBD)	nr_ar_lbd	Inactive	0.95
Tox21-Nuclear receptor signalling pathways	Aromatase	nr_aromatase	Inactive	0.98
Tox21-Nuclear receptor signalling pathways	Estrogen Receptor Alpha (ER)	nr_er	Inactive	0.97
Tox21-Nuclear receptor signalling pathways	Estrogen Receptor Ligand Binding Domain (ER-LBD)	nr_er_lbd	Inactive	0.99
Tox21-Nuclear receptor signalling pathways	Peroxisome Proliferator Activated Receptor Gamma (PPAR-Gamma)	nr_ppar_gamma	Inactive	0.93
Tox21-Stress response pathways	Nuclear factor (erythroid-derived 2)-like 2/antioxidant responsive element (nrf2/ARE)	sr_are	Inactive	0.95
Tox21-Stress response pathways	Heat shock factor response element (HSE)	sr_hse	Inactive	0.95
Tox21-Stress response pathways	Mitochondrial Membrane Potential (MMP)	sr_mmp	Inactive	0.84
Tox21-Stress response pathways	Phosphoprotein (Tumor Suppressor) p53	sr_p53	Inactive	0.91
Tox21-Stress response pathways	ATPase family AAA domain-containing protein 5 (ATAD5)	sr_atad5	Inactive	0.99

(B)

**Figure 25S.** Physical characters (A) and Toxicity Model Report (B) for compound 5.

Molweight	470.46
Number of hydrogen bond acceptors	28
Number of hydrogen bond donors	2
Number of atoms	51
Number of bonds	54
Number of rotatable bonds	7
Molecular refractivity	118.58
Topological Polar Surface Area	171.25
octanol/water partition coefficient(logP)	0.89

(A)

## Supplementary Materials

Classification	Target	Shorthand	Prediction	Probability
Organ toxicity	Hepatotoxicity	dili	Inactive	0.56
Toxicity end points	Carcinogenicity	carcino	Inactive	0.60
Toxicity end points	Immunotoxicity	immuno	Inactive	0.99
Toxicity end points	Mutagenicity	mutagen	Inactive	0.74
Toxicity end points	Cytotoxicity	cyto	Inactive	0.56
Tox21-Nuclear receptor signalling pathways	Aryl hydrocarbon Receptor (AhR)	nr_ahr	Inactive	0.92
Tox21-Nuclear receptor signalling pathways	Androgen Receptor (AR)	nr_ar	Inactive	0.98
Tox21-Nuclear receptor signalling pathways	Androgen Receptor Ligand Binding Domain (AR-LBD)	nr_ar_lbd	Inactive	0.97
Tox21-Nuclear receptor signalling pathways	Aromatase	nr_aromatase	Inactive	0.98
Tox21-Nuclear receptor signalling pathways	Estrogen Receptor Alpha (ER)	nr_er	Inactive	0.97
Tox21-Nuclear receptor signalling pathways	Estrogen Receptor Ligand Binding Domain (ER-LBD)	nr_er_lbd	Inactive	0.99
Tox21-Nuclear receptor signalling pathways	Peroxisome Proliferator Activated Receptor Gamma (PPAR-Gamma)	nr_ppar_gamma	Inactive	0.94
Tox21-Stress response pathways	Nuclear factor (erythroid-derived 2)-like 2/antioxidant responsive element (nrf2/ARE)	sr_are	Inactive	0.95
Tox21-Stress response pathways	Heat shock factor response element (HSE)	sr_hse	Inactive	0.95
Tox21-Stress response pathways	Mitochondrial Membrane Potential (MMP)	sr_mmp	Inactive	0.88
Tox21-Stress response pathways	Phosphoprotein (Tumor Suppressor) p53	sr_p53	Inactive	0.91
Tox21-Stress response pathways	ATPase family AAA domain-containing protein 5 (ATAD5)	sr_atad5	Inactive	0.99

(B)

**Figure 26S.** Physical characteristics (A) and Toxicity Model Report (B) for compound **9a**

Molweight	404.4
Number of hydrogen bond acceptors	24
Number of hydrogen bond donors	2
Number of atoms	44
Number of bonds	47
Number of rotatable bonds	2
Molecular refractivity	104.2
Topological Polar Surface Area	153.83
octanol/water partition coefficient(logP)	1.48

(A)



## Supplementary Materials

Classification	Target	Shorthand	Prediction	Probability
Organ toxicity	Hepatotoxicity	dili	Active	0.50
Toxicity end points	Carcinogenicity	carcino	Inactive	0.62
Toxicity end points	Immunotoxicity	immuno	Inactive	0.98
Toxicity end points	Mutagenicity	mutagen	Inactive	0.75
Toxicity end points	Cytotoxicity	cyto	Inactive	0.60
Tox21-Nuclear receptor signalling pathways	Aryl hydrocarbon Receptor (AhR)	nr_ahr	Inactive	0.96
Tox21-Nuclear receptor signalling pathways	Androgen Receptor (AR)	nr_ar	Inactive	0.97
Tox21-Nuclear receptor signalling pathways	Androgen Receptor Ligand Binding Domain (AR-LBD)	nr_ar_lbd	Inactive	0.97
Tox21-Nuclear receptor signalling pathways	Aromatase	nr_aromatase	Inactive	0.96
Tox21-Nuclear receptor signalling pathways	Estrogen Receptor Alpha (ER)	nr_er	Inactive	0.95
Tox21-Nuclear receptor signalling pathways	Estrogen Receptor Ligand Binding Domain (ER-LBD)	nr_er_lbd	Inactive	1.0
Tox21-Nuclear receptor signalling pathways	Peroxisome Proliferator Activated Receptor Gamma (PPAR-Gamma)	nr_ppar_gamma	Inactive	0.96
Tox21-Stress response pathways	Nuclear factor (erythroid-derived 2)-like 2/antioxidant responsive element (nrf2/ARE)	sr_are	Inactive	0.99
Tox21-Stress response pathways	Heat shock factor response element (HSE)	sr_hse	Inactive	0.99
Tox21-Stress response pathways	Mitochondrial Membrane Potential (MMP)	sr_mmp	Inactive	0.86
Tox21-Stress response pathways	Phosphoprotein (Tumor Suppressor) p53	sr_p53	Inactive	0.92
Tox21-Stress response pathways	ATPase family AAA domain-containing protein 5 (ATAD5)	sr_atad5	Inactive	0.99

(B)

**Figure 27S.** Physical characteristics (A) and Toxicity Model Report (B) for compound **19**

Molweight	602.58
Number of hydrogen bond acceptors	48
Number of hydrogen bond donors	4
Number of atoms	77
Number of bonds	80
Number of rotatable bonds	14
Molecular refractivity	150.43
Topological Polar Surface Area	213.36
octanol/water partition coefficient(logP)	3.28

(A)

## Supplementary Materials

Classification	Target	Shorthand	Prediction	Probability
Organ toxicity	Hepatotoxicity	dili	Inactive	0.56
Toxicity end points	Carcinogenicity	carcino	Inactive	0.55
Toxicity end points	Immunotoxicity	immuno	Inactive	0.90
Toxicity end points	Mutagenicity	mutagen	Inactive	0.62
Toxicity end points	Cytotoxicity	cyto	Inactive	0.55
Tox21-Nuclear receptor signalling pathways	Aryl hydrocarbon Receptor (AhR)	nr_ahr	Inactive	0.86
Tox21-Nuclear receptor signalling pathways	Androgen Receptor (AR)	nr_ar	Inactive	0.97
Tox21-Nuclear receptor signalling pathways	Androgen Receptor Ligand Binding Domain (AR-LBD)	nr_ar_lbd	Inactive	0.93
Tox21-Nuclear receptor signalling pathways	Aromatase	nr_aromatase	Inactive	0.90
Tox21-Nuclear receptor signalling pathways	Estrogen Receptor Alpha (ER)	nr_er	Inactive	0.89
Tox21-Nuclear receptor signalling pathways	Estrogen Receptor Ligand Binding Domain (ER-LBD)	nr_er_lbd	Inactive	0.97
Tox21-Nuclear receptor signalling pathways	Peroxisome Proliferator Activated Receptor Gamma (PPAR-Gamma)	nr_ppar_gamma	Inactive	0.95
Tox21-Stress response pathways	Nuclear factor (erythroid-derived 2)-like 2/antioxidant responsive element (nrf2/ARE)	sr_are	Inactive	0.93
Tox21-Stress response pathways	Heat shock factor response element (HSE)	sr_hse	Inactive	0.93
Tox21-Stress response pathways	Mitochondrial Membrane Potential (MMP)	sr_mmp	Inactive	0.77
Tox21-Stress response pathways	Phosphoprotein (Tumor Suppressor) p53	sr_p53	Inactive	0.81
Tox21-Stress response pathways	ATPase family AAA domain-containing protein 5 (ATAD5)	sr_atad5	Inactive	0.86

(B)

**Figure 28S.** Physical characteristics (A) and Toxicity Model Report (B) for **Remdesivir**

Molweight	157.1
Number of hydrogen bond acceptors	8
Number of hydrogen bond donors	2
Number of atoms	15
Number of bonds	15
Number of rotatable bonds	1
Molecular refractivity	32.91
Topological Polar Surface Area	88.84
octanol/water partition coefficient(logP)	-0.29

(A)

## Supplementary Materials

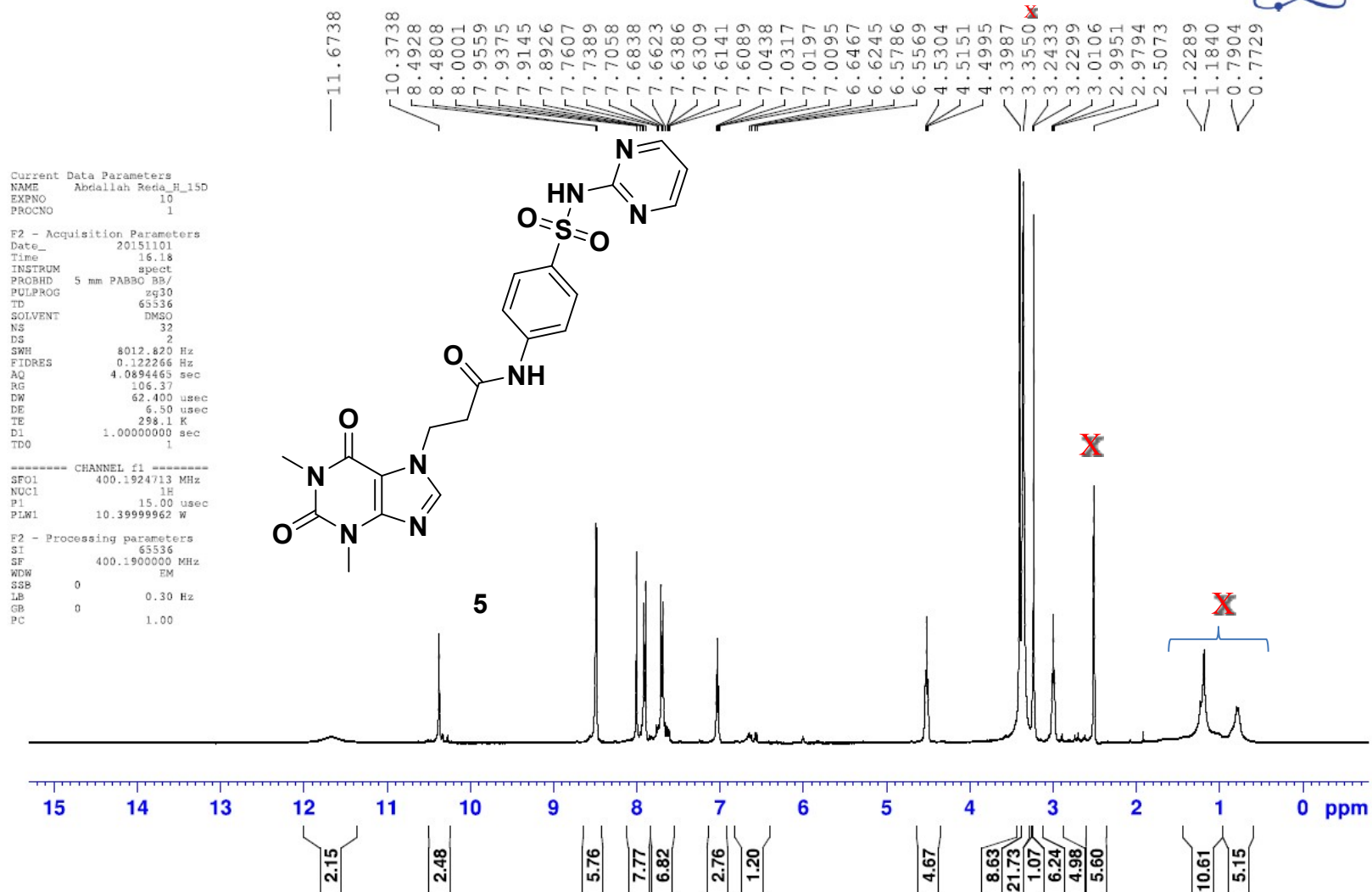
Classification	Target	Shorthand	Prediction	Probability
Organ toxicity	Hepatotoxicity	dili	Inactive	0.66
Toxicity end points	Carcinogenicity	carcino	Active	0.53
Toxicity end points	Immunotoxicity	immuno	Inactive	0.99
Toxicity end points	Mutagenicity	mutagen	Inactive	0.76
Toxicity end points	Cytotoxicity	cyto	Inactive	0.84
Tox21-Nuclear receptor signalling pathways	Aryl hydrocarbon Receptor (AhR)	nr_ahr	Inactive	0.82
Tox21-Nuclear receptor signalling pathways	Androgen Receptor (AR)	nr_ar	Inactive	0.97
Tox21-Nuclear receptor signalling pathways	Androgen Receptor Ligand Binding Domain (AR-LBD)	nr_ar_lbd	Inactive	0.99
Tox21-Nuclear receptor signalling pathways	Aromatase	nr_aromatase	Inactive	0.97
Tox21-Nuclear receptor signalling pathways	Estrogen Receptor Alpha (ER)	nr_er	Inactive	0.95
Tox21-Nuclear receptor signalling pathways	Estrogen Receptor Ligand Binding Domain (ER-LBD)	nr_er_lbd	Inactive	0.97
Tox21-Nuclear receptor signalling pathways	Peroxisome Proliferator Activated Receptor Gamma (PPAR-Gamma)	nr_ppar_gamma	Inactive	0.99
Tox21-Stress response pathways	Nuclear factor (erythroid-derived 2)-like 2/antioxidant responsive element (nrf2/ARE)	sr_are	Inactive	0.96
Tox21-Stress response pathways	Heat shock factor response element (HSE)	sr_hse	Inactive	0.96
Tox21-Stress response pathways	Mitochondrial Membrane Potential (MMP)	sr_mmp	Inactive	0.89
Tox21-Stress response pathways	Phosphoprotein (Tumor Suppressor) p53	sr_p53	Inactive	0.50
Tox21-Stress response pathways	ATPase family AAA domain-containing protein 5 (ATAD5)	sr_atad5	Inactive	0.58

(B)

**Figure 29S.** Physical characteristics (A) and Toxicity Model Report (B) for Favipiravir

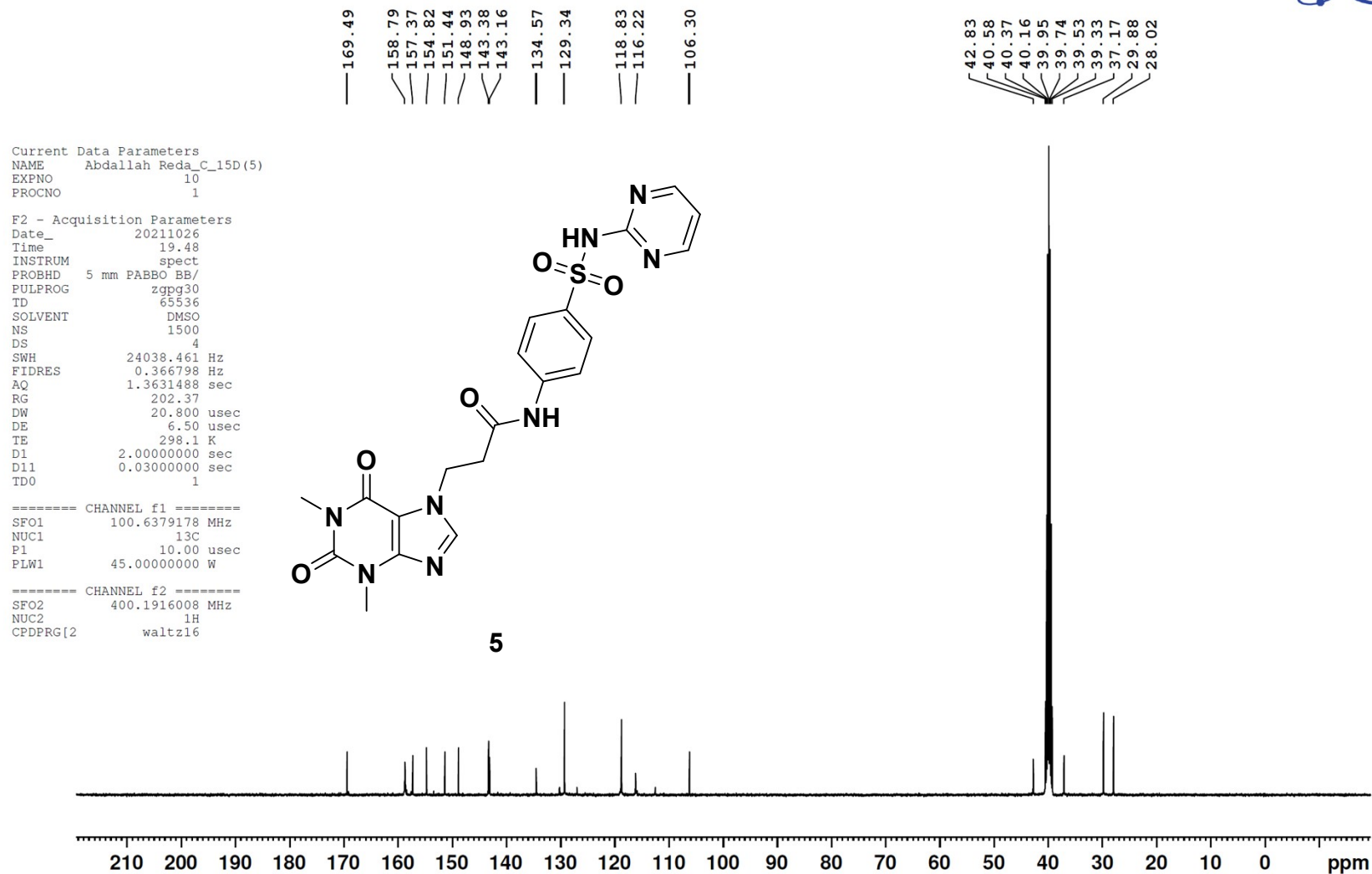
**7. Spectral data**

Abdallah Reda\_H\_15D

Microanalytical Unit - FOPCU - NMR laboratory  
www.pharma.cu.edu.eg dir-mau.fopcu@pharma.cu.edu.eg

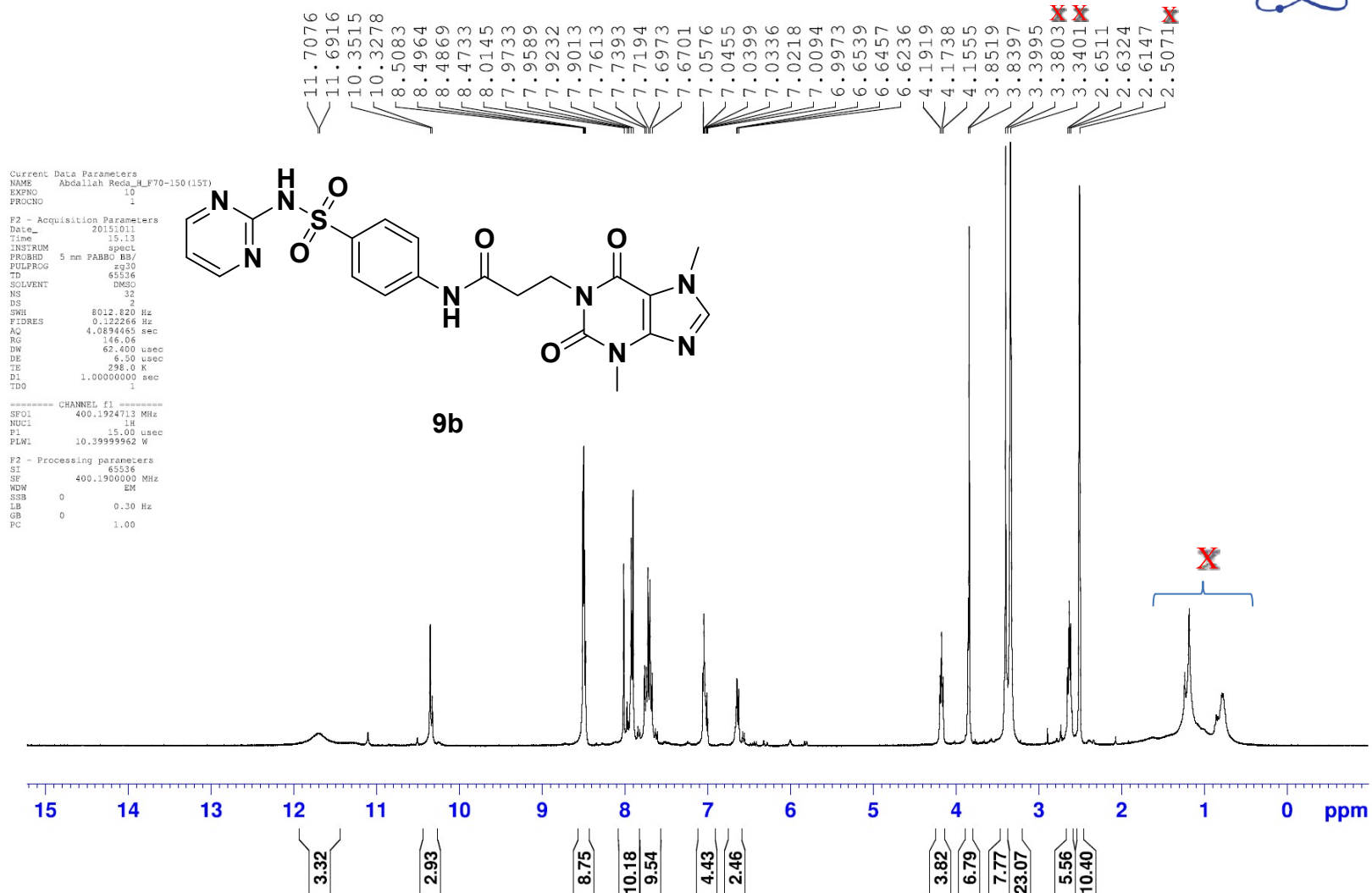
X are signals of DMSO, water and/or solvent residues

Abdallah Reda\_C\_15D(5)

Microanalytical Unit - FOPCU - NMR laboratory  
www.pharma.cu.edu.eg dir-mau.fopcu@pharma.cu.edu.eg

Abdallah Reda\_H\_F70-150 (15T)

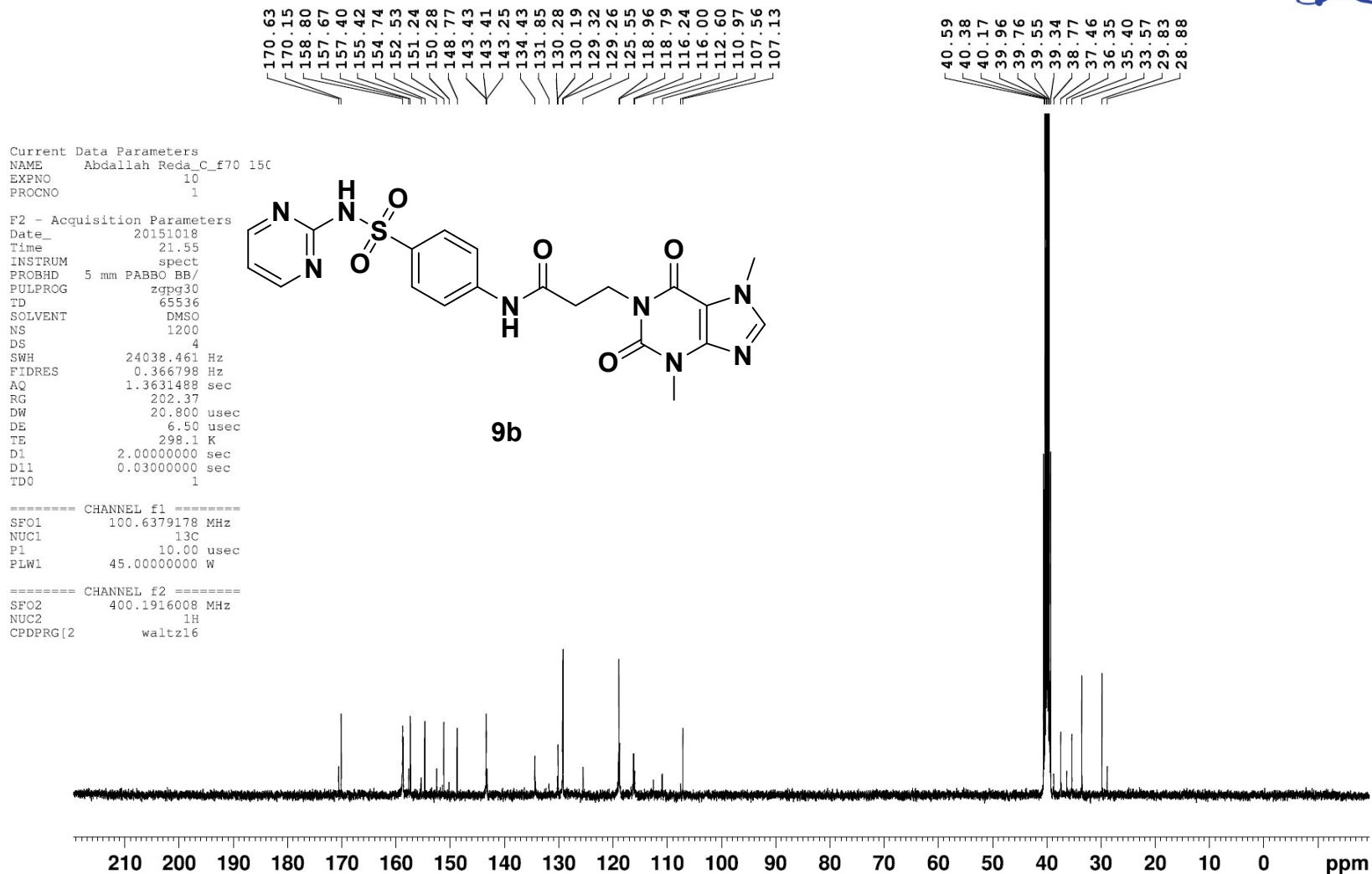
Microanalytical Unit - FOPCU - NMR laboratory  
www.pharma.cu.edu.eg dir-mau.fopcu@pharma.cu.edu.eg



X are signals of DMSO, water and/or solvent residues



Abdallah Reda\_C\_f70 150 (15T)





Abdallah Reda\_1E\_H

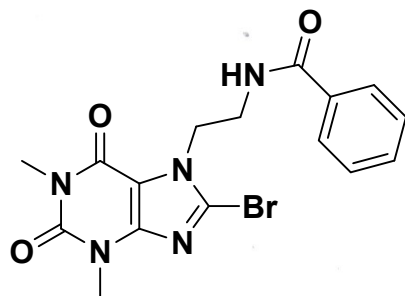
Microanalytical Unit - FOPCU  
NMR laboratory

Current Data Parameters  
NAME Abdallah Reda\_1E\_H  
EXPNO 10  
PROCNO 1

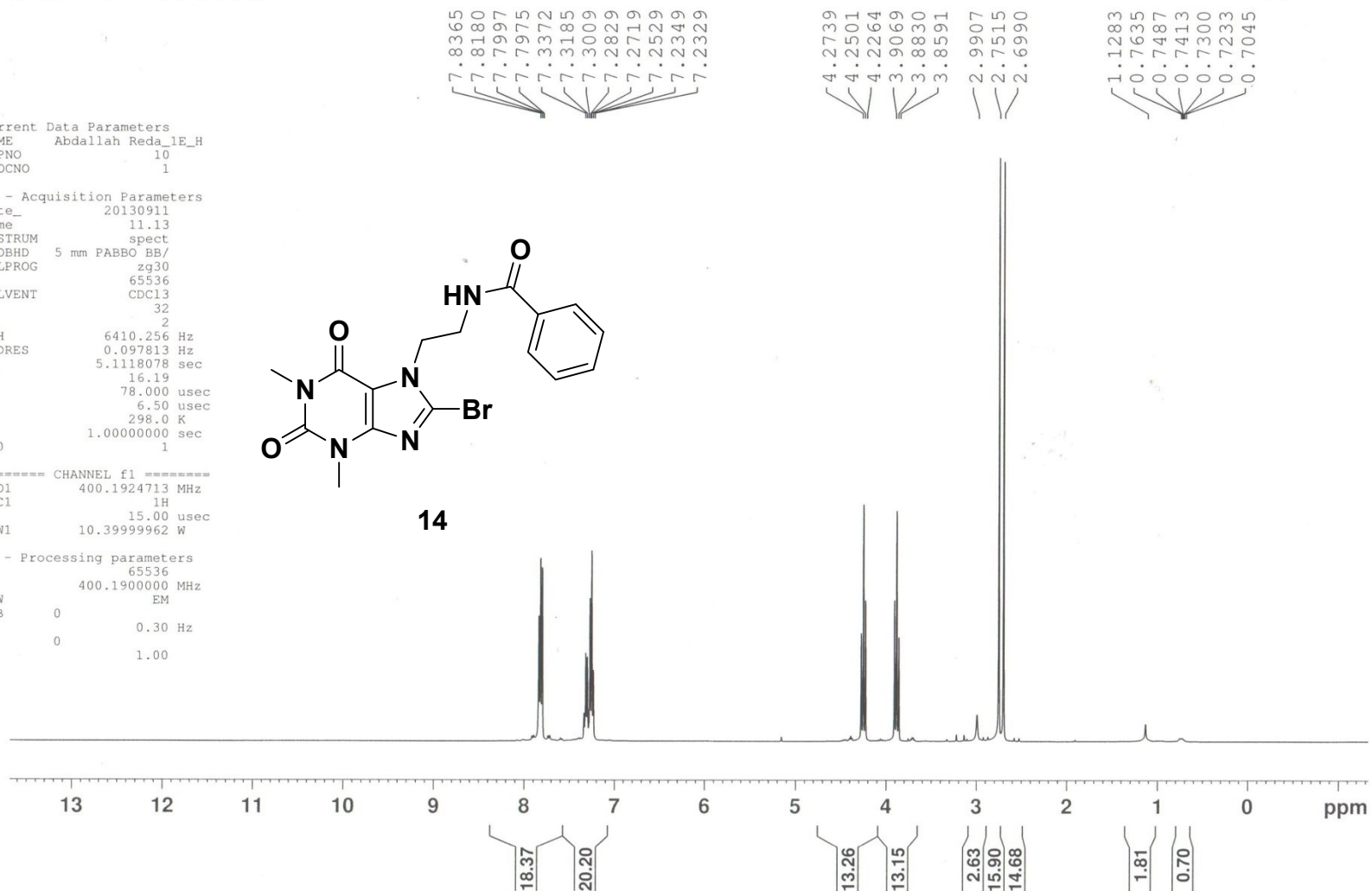
F2 - Acquisition Parameters  
Date\_ 20130911  
Time 11.13  
INSTRUM spect  
PROBHD 5 mm PABBO BB/  
PULPROG zg30  
TD 65536  
SOLVENT CDCl3  
NS 32  
DS 2  
SWH 6410.256 Hz  
FIDRES 0.097813 Hz  
AQ 5.1118078 sec  
RG 16.19  
DW 78.000 usec  
DE 6.50 usec  
TE 298.0 K  
D1 1.0000000 sec  
TD0 1

----- CHANNEL f1 -----  
SFO1 400.1924713 MHz  
NUC1 1H  
P1 15.00 usec  
PLW1 10.39999962 W

F2 - Processing parameters  
SI 65536  
SF 400.1900000 MHz  
WDW EM  
SSB 0  
LB 0.30 Hz  
GB 0  
PC 1.00



14



## Abdallah Reda\_C\_1E(14)

Microanalytical Unit - FOPCU - NMR laboratory  
www.pharma.cu.edu.eg dir-mau.fopcu@pharma.cu.edu.eg



168.63  
167.97  
167.06

134.15  
133.32  
131.64  
131.58  
129.69  
128.61  
128.53  
128.48  
127.05  
126.98

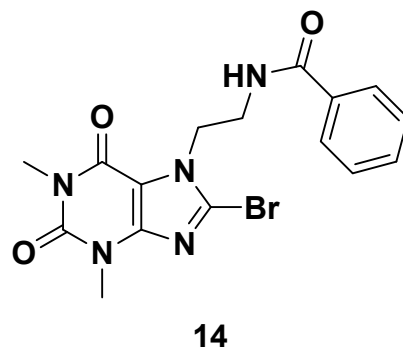
77.39  
77.08  
76.76

63.75  
61.99

42.85  
39.74

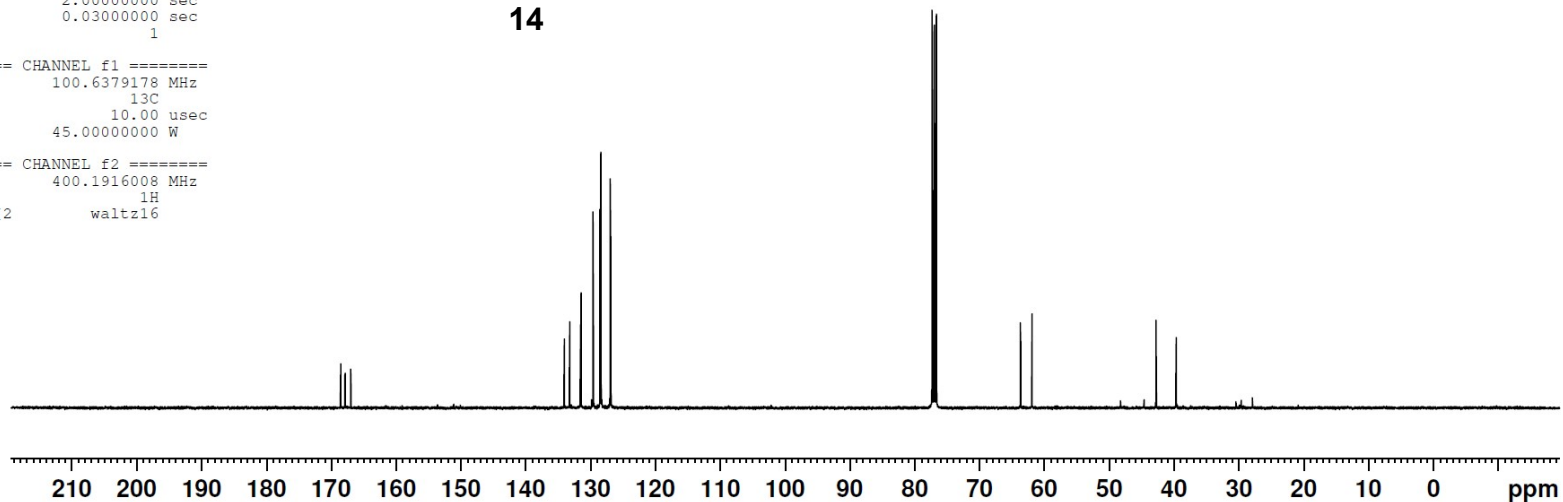
Current Data Parameters  
NAME Abdallah Reda\_C\_1E(14)  
EXPNO 10  
PROCNO 1

F2 - Acquisition Parameters  
Date\_ 20211027  
Time 1.43  
INSTRUM spect  
PROBHD 5 mm PABBO BB/  
PULPROG zgpg30  
TD 65536  
SOLVENT CDCl3  
NS 1500  
DS 4  
SWH 24038.461 Hz  
FIDRES 0.366798 Hz  
AQ 1.3631488 sec  
RG 202.37  
DW 20.800 usec  
DE 6.50 usec  
TE 298.0 K  
D1 2.00000000 sec  
D11 0.03000000 sec  
TD0 1

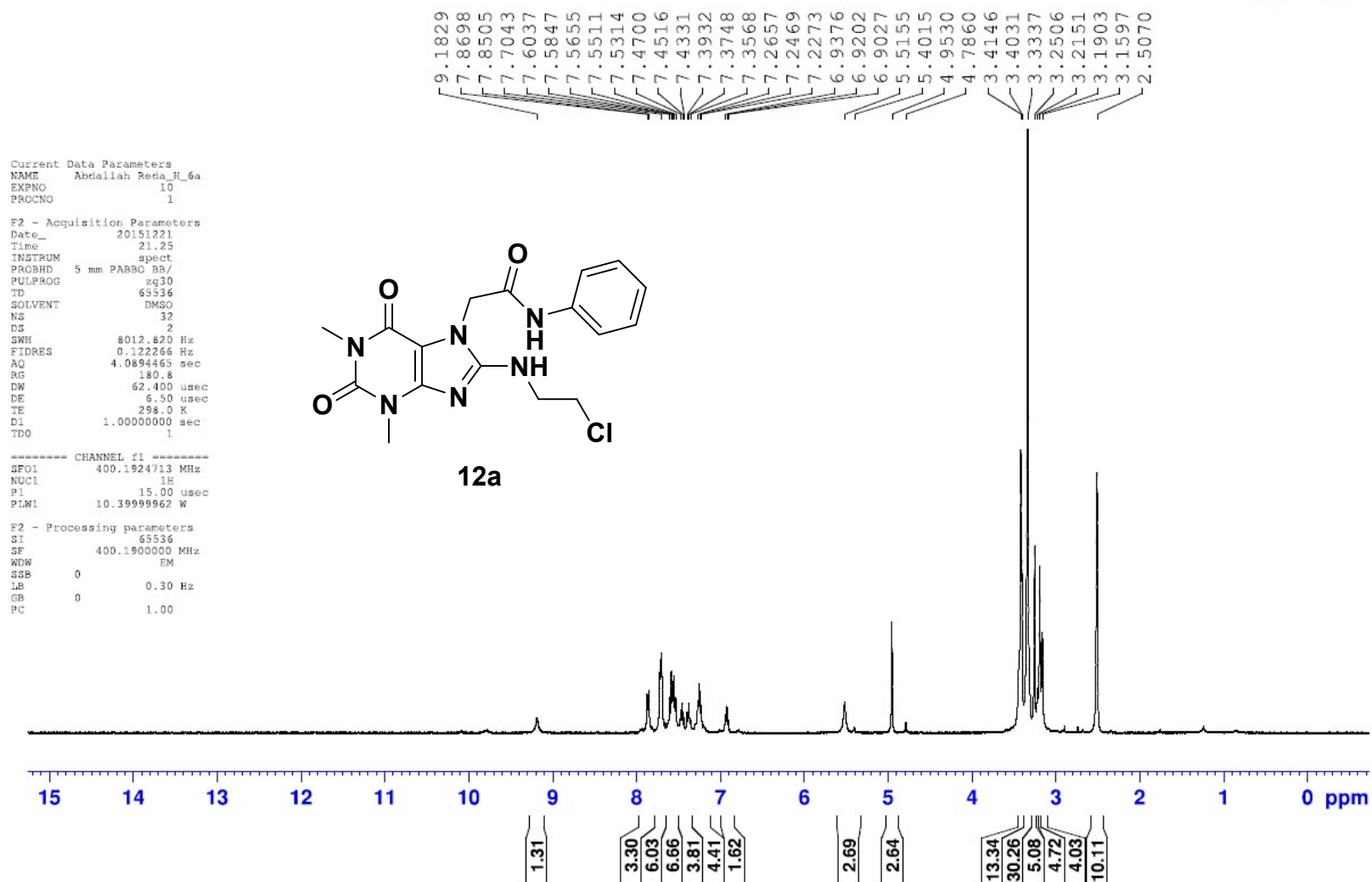


==== CHANNEL f1 =====  
SFO1 100.6379178 MHz  
NUC1 13C  
P1 10.00 usec  
PLW1 45.00000000 W

==== CHANNEL f2 =====  
SFO2 400.1916008 MHz  
NUC2 1H  
CPDPRG[2] waltz16



Abdallah Reda\_H\_6a

Microanalytical Unit - FOPCU - NMR laboratory  
www.pharma.cu.edu.eg dir-mau.fopcu@pharma.cu.edu.eg

Abdallah Reda\_C\_6a

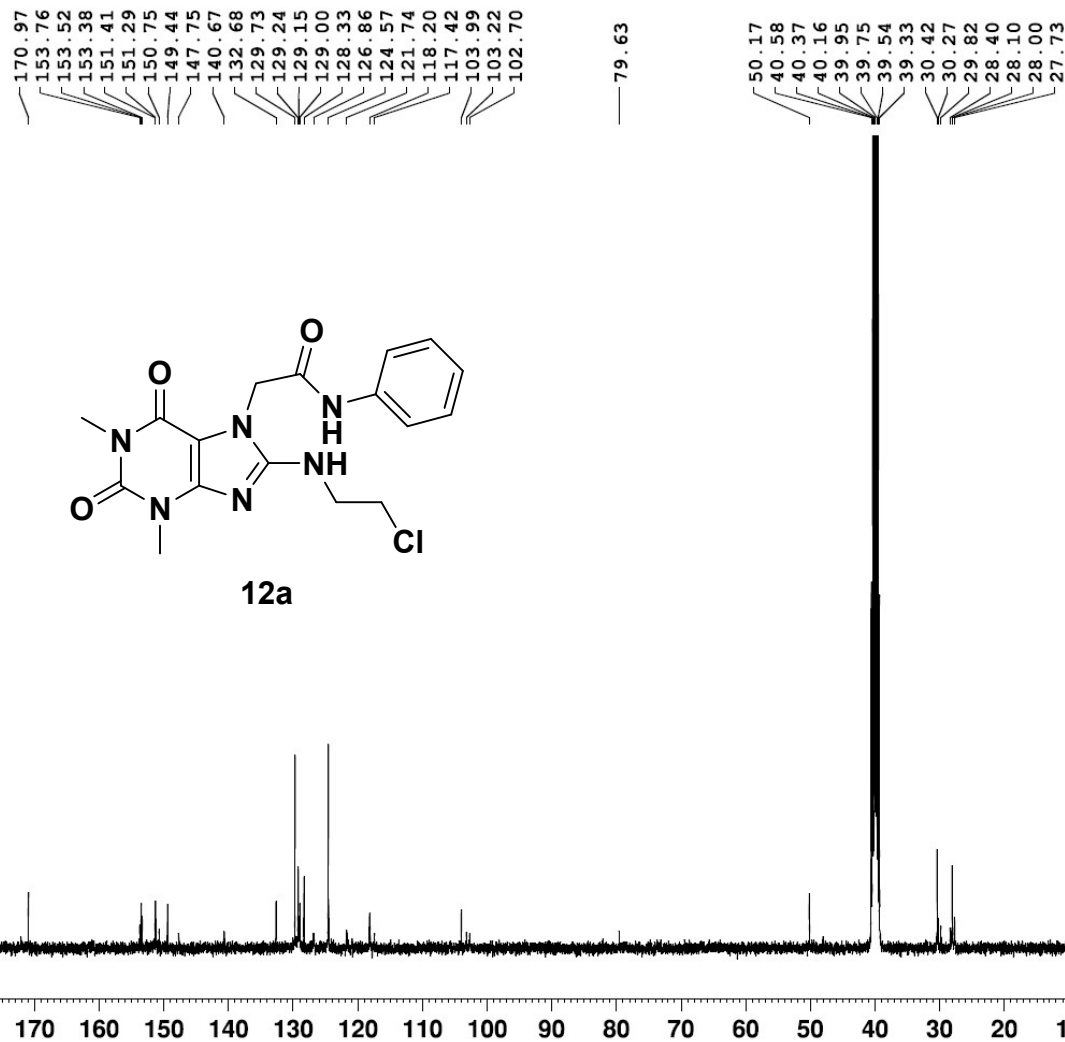
Microanalytical Unit - FOPCU - NMR laboratory  
www.pharma.cu.edu.eg dir-mau.fopcu@pharma.cu.edu.eg

Current Data Parameters  
NAME Abdallah Reda\_C\_6a  
EXPNO 10  
PROCNO 1

F2 - Acquisition Parameters  
Date\_ 20160111  
Time 8.23  
INSTRUM spect  
PROBHD 5 mm PABBO BB/  
PULPROG zgpg30  
TD 65536  
SOLVENT DMSO  
NS 1200  
DS 4  
SWH 24038.461 Hz  
FIDRES 0.366798 Hz  
AQ 1.3631488 sec  
RG 202.37  
DW 20.800 usec  
DE 6.50 usec  
TE 298.1 K  
D1 2.00000000 sec  
D11 0.03000000 sec  
TD0 1

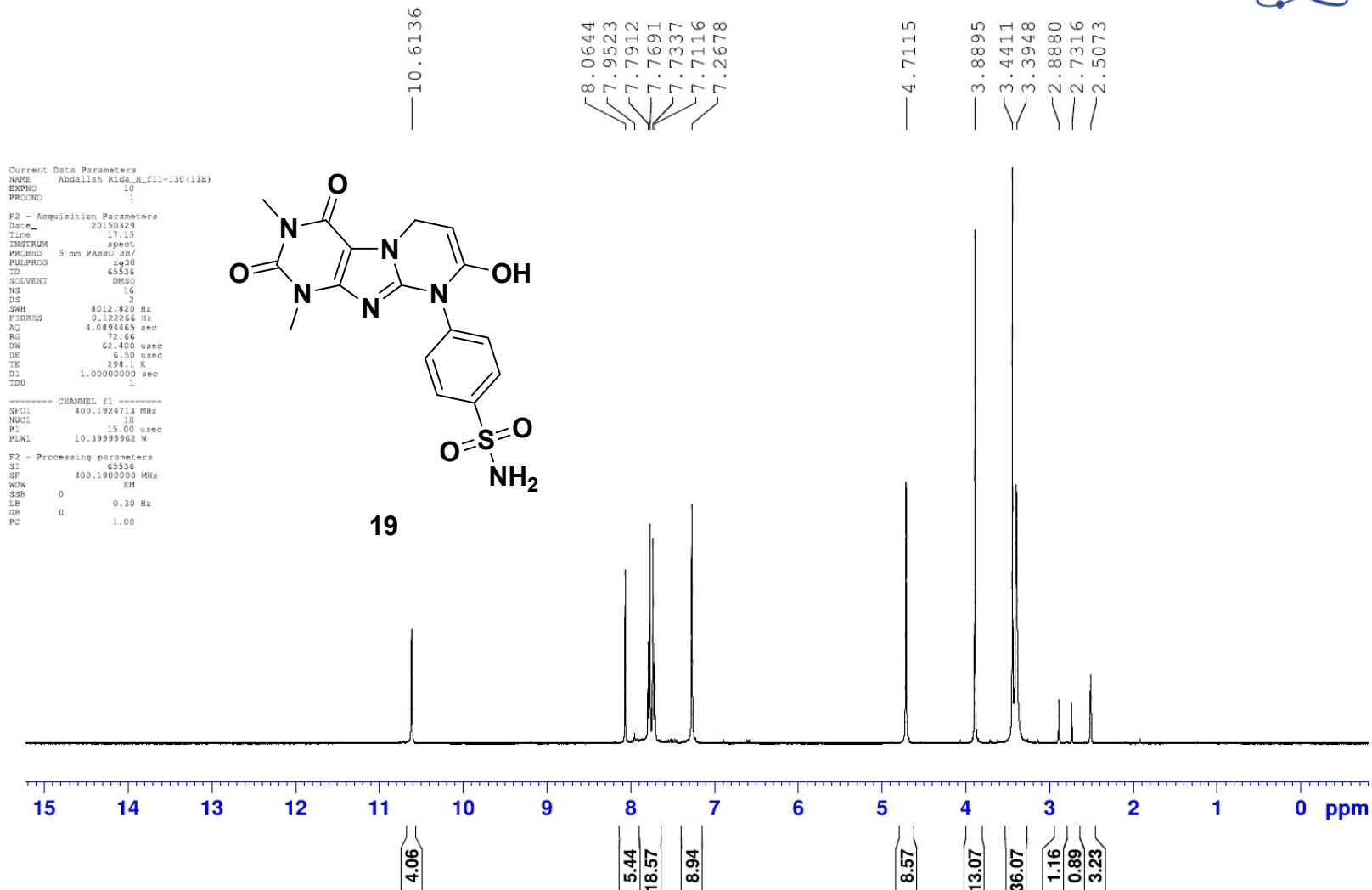
===== CHANNEL f1 =====  
SFO1 100.6379178 MHz  
NUC1 13C  
P1 10.00 usec  
PLW1 45.00000000 W

===== CHANNEL f2 =====  
SFO2 400.1916008 MHz  
NUC2 1H  
CPDPRG[2] waltz16

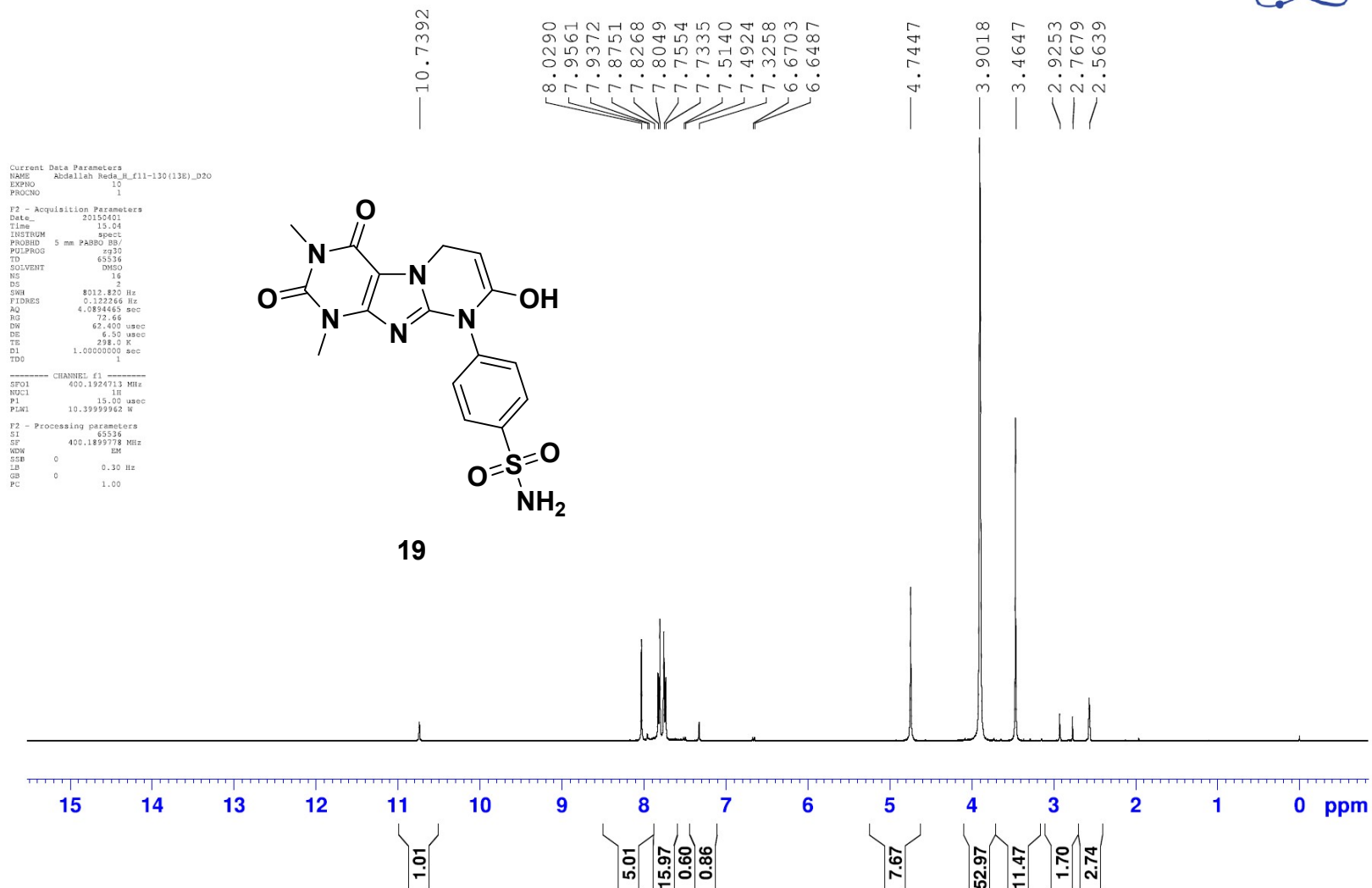


Abdallah Rida\_H\_f11-130 (13E)

Microanalytical Unit - FOPCU - NMR laboratory  
www.pharma.cu.edu.eg dir-mau.fopcu@pharma.cu.edu.eg

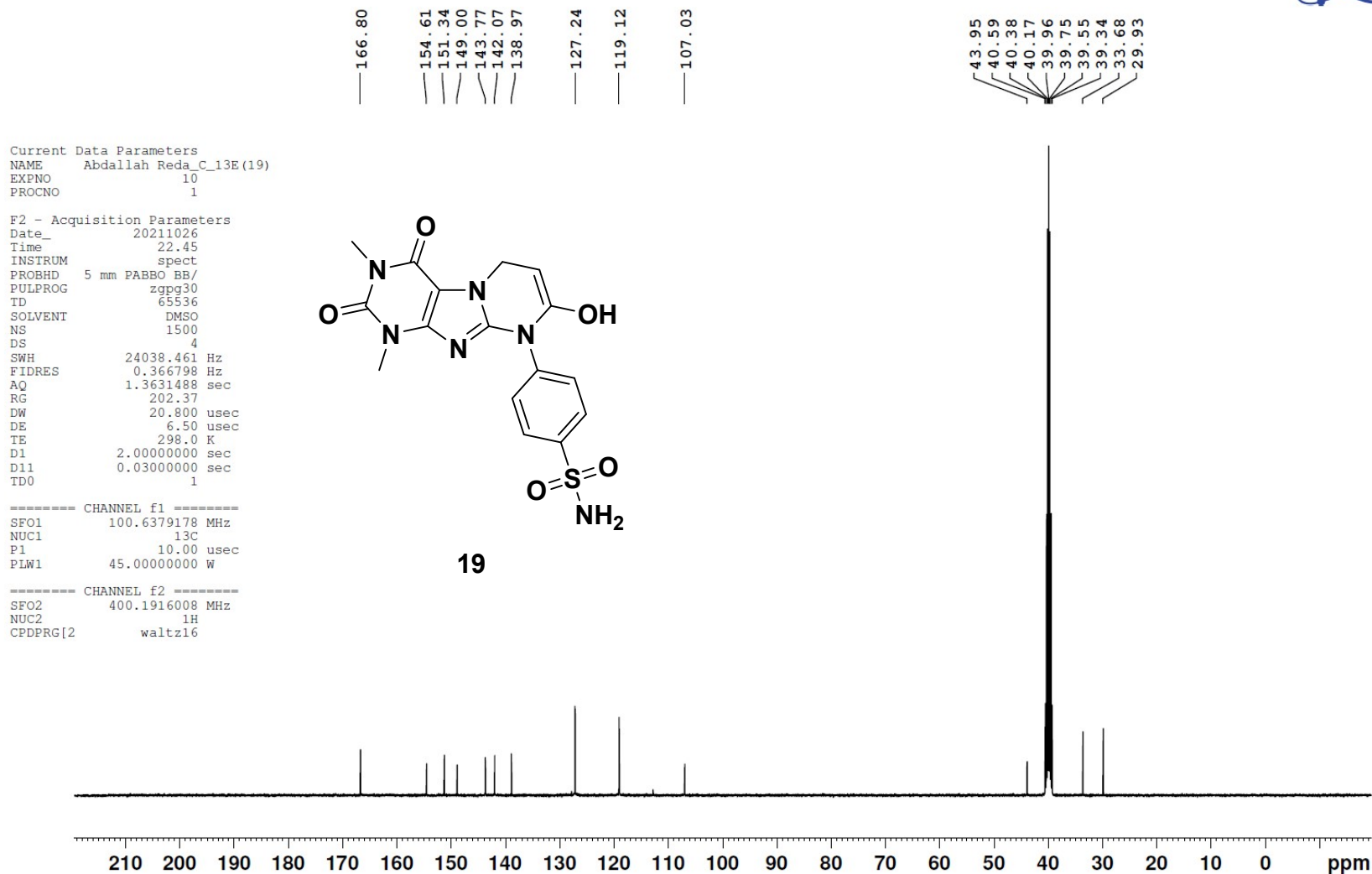


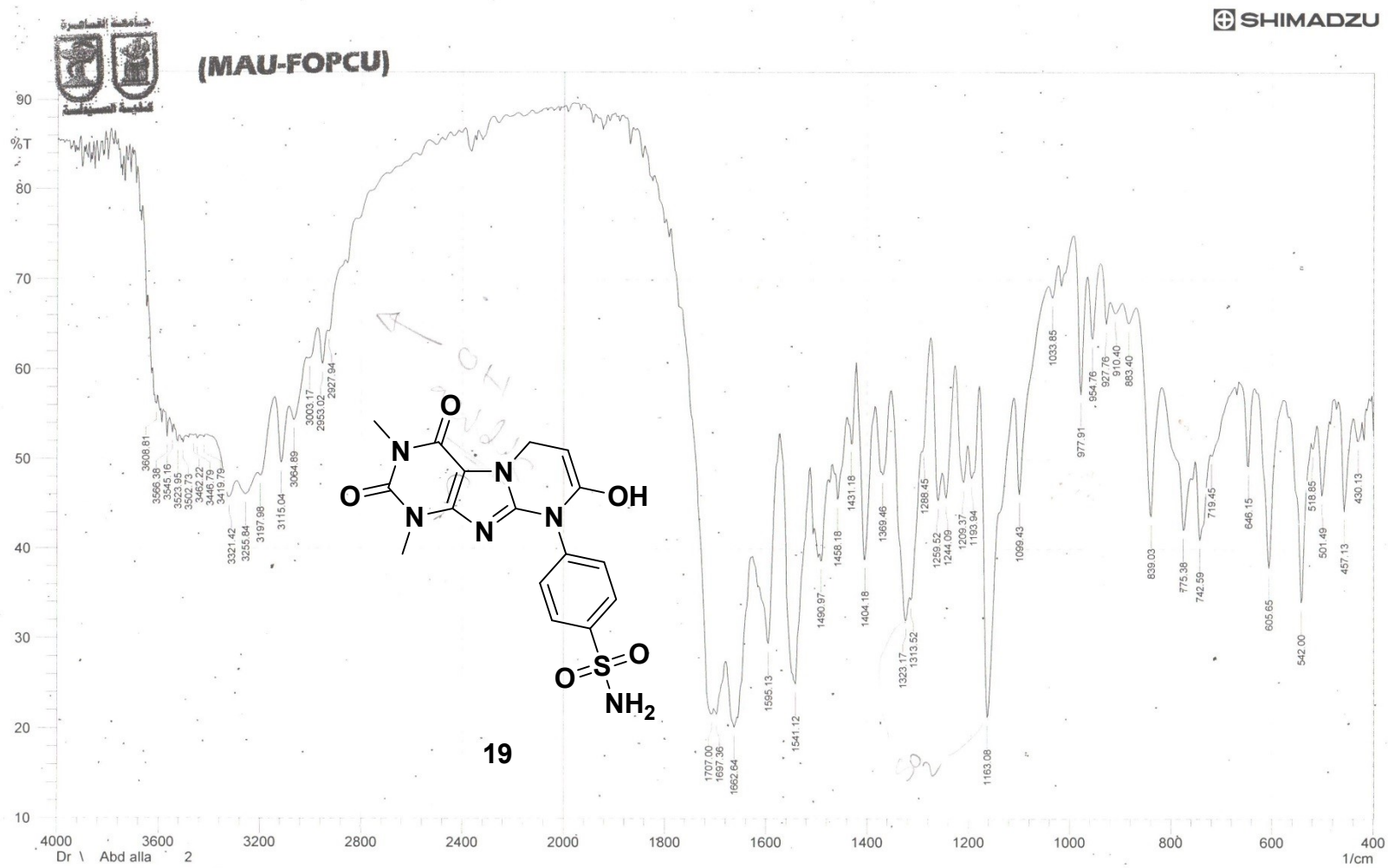
Abdallah Reda\_H\_f11-130 (13E)\_D2O

Microanalytical Unit - FOPCU - NMR laboratory  
www.pharma.cu.edu.eg dir-mau.fopcu@pharma.cu.edu.eg

## Abdallah Reda\_C\_13E(19)

Microanalytical Unit - FOPCU - NMR laboratory  
www.pharma.cu.edu.eg dir-mau.fopcu@pharma.cu.edu.eg





Comment;

Dr \ Abd alla 2

\*\*\*  
(4h2)  
11.130 (13E)  
(12F?)

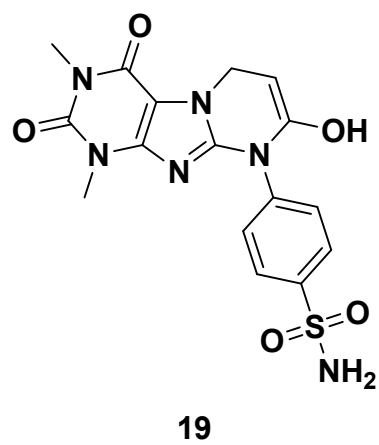
No. of Scans; 8

Resolution; 4 [1/cm]

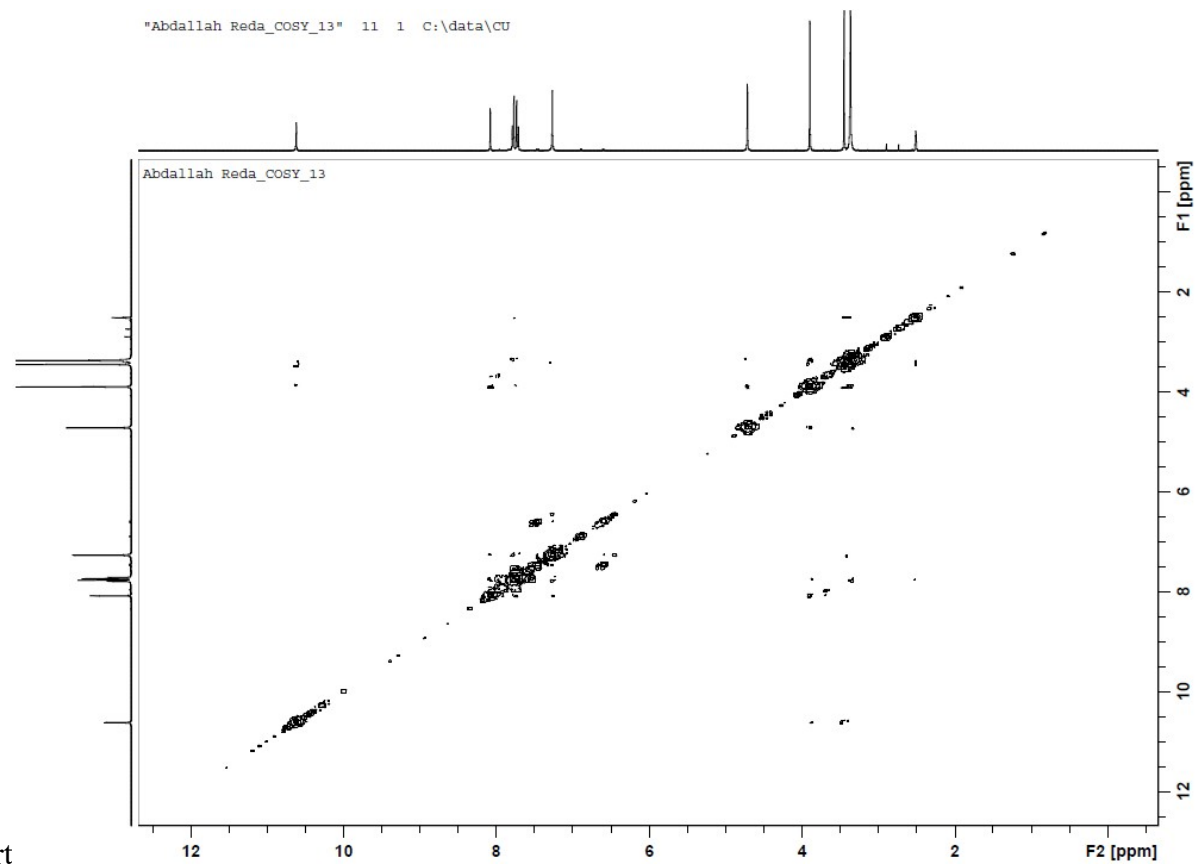
Date/Time; 3/22/2015 9:50:16 AM

User; user





$^1\text{H}$ - $^1\text{H}$  COSY, 2D-NMR chart



## References

- [1] C. Legler, N. Brown, R. Dunbar, M. Harness, K. Nguyen, O. Oyewole, W. Collier. Scaled quantum mechanical scale factors for vibrational calculations using alternate polarized and augmented basis sets with the B3LYP density functional calculation model, *Spectrochim. Acta - A: Mol. Biomol.*, 145 (2015) 15-24.
- [2] A.M. Dhumad, H.J. Majeed, K. Harismah, H. Zandi. In silico approach on ribavirin inhibitors for COVID-19 main protease, *Biointerface Res. Appl. Chem.*, 11 (2021) 13924-13933.
- [3] P. Yadav, M. Rana, P. Chowdhury. DFT and MD simulation investigation of favipiravir as an emerging antiviral option against viral protease (3CLpro) of SARS-CoV-2, *J. Mol. Struct.*, 1246 (2021) 131253.
- [4] R. Kumari, R. Kumar, A. Lynn. g\_mmpbsa. A GROMACS tool for high-throughput MM-PBSA calculations, *J. Chem. Inf. Model*, 54 (2014) 1951-1962.
- [5] W. Humphrey, A. Dalke, K. Schulten. VMD: visual molecular dynamics, *J. Mol. Graph.*, 14 (1996) 33-38.
- [6] M.N. Drwal, P. Banerjee, M. Dunkel, M.R. Wettig, R. Preissner. ProTox: a web server for the in silico prediction of rodent oral toxicity, *Nucleic Acids Res.*, 42 (2014) W53-W58.